Fall 1-31-2014

Influence of lateral boundaries in tapped densification of granular materials

Nathaniel Ching
New Jersey Institute of Technology

Copyright Warning & Restrictions

The copyright law of the United States (Title 17, United States Code) governs the making of photocopies or other reproductions of copyrighted material.

Under certain conditions specified in the law, libraries and archives are authorized to furnish a photocopy or other reproduction. One of these specified conditions is that the photocopy or reproduction is not to be "used for any purpose other than private study, scholarship, or research." If a, user makes a request for, or later uses, a photocopy or reproduction for purposes in excess of "fair use" that user may be liable for copyright infringement,

This institution reserves the right to refuse to accept a copying order if, in its judgment, fulfillment of the order would involve violation of copyright law.

Please Note: The author retains the copyright while the New Jersey Institute of Technology reserves the right to distribute this thesis or dissertation

Printing note: If you do not wish to print this page, then select "Pages from: first page # to: last page #" on the print dialog screen

ABSTRACT

INFLUENCE OF LATERAL BOUNDARIES IN TAPPED DENSIFICATION OF GRANULAR MATERIALS

by
Nathaniel Ching

Granular systems are widely present in the world. Soil, pharmaceutical pills, and silos filled with grain all are examples of granular systems. Experiments have long established an empirical understanding of granular systems, but an analytical understanding has been much more difficult to establish. One of the behaviors of a granular system that is well documented but poorly understood is the change in density the system undergoes when excited, also known as the densification process.

This thesis investigates the densification process of a tapped granular system using Discrete Element Model (DEM) simulations. Contact interactions in the simulations obey a well-established inelastic soft-sphere model. The computational volume consists of a rectangular parallelepiped with a square base that is 12 particle diameters wide and filled with 3456 spheres. A focus of this work is on understanding the influence of the walls on the densification process.

Several systems are observed to stay in a metastable state for thousands of taps before further densification occurs. In addition, bulk lateral movement or drift of the sphere assembly is detected after evolving to maximally dense state, even though the particles come to a complete rest between taps. Simulations conducted with solid lateral walls suggest a reduced rate of densification as compared to the periodic systems, which is hypothesized to be caused in part by a motion restriction of the spheres imposed by the solid walls.

INFLUENCE OF LATERAL BOUNDARIES IN TAPPED DENSIFICATION OF GRANULAR MATERIALS

by
Nathaniel Ching

A Thesis
Submitted to the Faculty of
New Jersey Institute of Technology
in Partial Fulfillment of the Requirements for the Degree of
Master of Science in Mechanical Engineering

Department of Mechanical and Industrial Engineering

January 2014

APPROVAL PAGE

INFLUENCE OF LATERAL BOUNDARIES IN TAPPED DENSIFICATION OF GRANULAR MATERIALS

Nathaniel Ching

Dr. Anthony D. Rosato, Thesis Advisor — Date
Professor of Mechanical Engineering, NJIT

Dr. Pushpendra Singh, Committee Member — Date
Professor of Mechanical Engineering, NJIT

Dr. Shawn A. Chester, Committee Member — Date
Assistant Professor of Mechanical Engineering, NJIT

Dr. David J. Horntrop, Committee Member — Date
Associate Professor of Mathematics, NJIT

BIOGRAPHICAL SKETCH

Author: Nathaniel Ching

Degree: Master of Science

Date: January 2014

Undergraduate and Graduate Education:

- Master of Science in Mechanical Engineering,
  New Jersey Institute of Technology, Newark, NJ, 2014
- Bachelor of Science in Mechanical Engineering,
  New Jersey Institute of Technology, Newark, NJ, 2011

Major: Mechanical Engineering

Publications:

V. Ratnaswamy, A. D. Rosato, D. Blackmore, X. Tricoche, N. Ching, and L. Zuo, "Evolution of solids fraction surfaces in tapping: simulation and dynamical systems analysis," *Granular Matter*, vol. 14, no. 2, pp. 163-168, 2012.

To my parents.

ACKNOWLEDGMENT

I would like to express sincere gratitude to my advisor, Dr. Anthony Rosato, for his support and guidance throughout my years of research. Special thanks go to my committee members: Dr. Pushpendra Singh, Dr. Shawn Chester, and Dr. David Horntrop. Some funding came from the NSF grant CMMI-1029809. Computing resources were provided by the NJIT High Performance Computing cluster named Kong. In addition, my fellow students Vishagan Ratnaswamy and Aleksandr Spiridonov were instrumental in helping me run the simulations and in modifying the simulation code.

TABLE OF CONTENTS

TABLE OF CONTENTS
(Continued)

Chapter **Page**

LIST OF TABLES

Table **Page**

LIST OF FIGURES

LIST OF FIGURES
(Continued)

Figure **Page**

CHAPTER 1

INTRODUCTION AND LITERATURE REVIEW

1.1 Introduction

Granular systems are widely used all over the modern world, and understanding the mechanics of granular systems can yield cheaper, stronger materials. The road we drive on, the engines in cars, the sand on the beach, plastic extrusion for smartphones, and the concrete building foundations all involve granular systems.

There are several areas of current research in the granular field. The arrangement of spheres in a dense state has been a mathematical problem of interest since 1611, when Kepler theorized that the Face-Centered-Cubic (FCC) pattern was the densest possible packing of spheres [1]. The Kepler Conjecture has not been formally proven, although Hales and Ferguson in 1998 published a preliminary proof [2], and research is ongoing to find a formal proof.

Another area of research is the field of granular flow, starting with the seminal research by Bagnold [3] and continuing to today. Practical examples are predicting the movement of silt in a waterway; chutes, silos, and valves that are used by the grain industry; and the understanding of landslides and avalanches. Yet another area of research is granular segregation under vibration, where mixed particles of different sizes and properties separate, has also been researched extensively. Granular segregation is applicable to all industries that mix and transport powders, sand, rocks, and other mixed granular material. Examples are the large chunks of cereal at the top of the box, or the separation of crushed ore on a moving conveyor belt. Granular segregation is also known as the Brazil Nut Effect [4] and the Reverse Brazil Nut Effect [5]. Other research has gone into powder mixing [6]. Powder mixing research explores how to best mix two granular materials, including mixing dissimilar materials while preventing

granular segregation from happening. A complex process of producing porous gold and other soft metals is based on completely mixing two dissimilar powders [6].

Research has also been done recently to form a continuum model to describe the granular systems. The continuum model can then be used in Finite Element Method (FEM) simulations. FEM simulations are much faster than the simulation methods used in this thesis because the FEM simulations do not have to track individual particles. Speed of computation makes FEM simulations much more useful for modeling industry problems described above with large numbers of particles. One mathematical model is to compare the granules in a system with molecules in a thermodynamic system. A granular system that keeps its structure during the vibrations is in the solid phase. If there is some movement, then it is a liquid. If there is a lot of movement, then the granular system is in the gas phase. Various methods of mapping variables in the granular system to thermodynamic variables have been explored [7]. The phase transitions of a granular system has also been explored [7]. Other models based on cellular automata and random walks have been proposed, as well as a model based on averaging of granular dynamics [8].

This thesis shall focus on the area of granular compaction under vibration and tapping. Research into the compaction of granular systems under vibration or tapping has deep practical implications. Powder metallurgy is one target of the research, as the strength and uniformity of the finished part is dependent on the uniformity of the powder before it is pressed or sintered [9]. The area of nuclear fuels manufacture was a special case of powder metallurgy that was researched in the 1960's [10]. A granular packing has a large surface area in comparison to even the roughest metal plates, so a granular metal anode or cathode with a low solids fraction can be used to create better batteries [11]. Additionally, complex shapes of molds for castings need to be made from dense, but porous materials. A sand mold that becomes denser during the pouring or injection of the metal will produce a deformed part. Vibration

or tapping is a standard method to compact the sand molds for casting before the metal is poured or injected [12].

Experiments with densification of granular systems are often done with an electromechanical shaker and a glass or acrylic tube. The electromechanical shaker allows the frequency and amplitude to be controlled precisely. The clear tube allows the researcher to measure the height, and therefore the density, of the system while it is being shaken. Sometimes, an experimenter will use the dielectric property of glass to measure the solids fraction of a specific area in a tube; the denser the system is, the higher the capacitance will be across the tube. Research in crystallography requires the experimenter to see the positions of the particles in the system. In order to see the positions of the particles inside a 3D system, the system could be filled with glue and then sliced, or the system could be put in an MRI scanner.

Early simulations were done with Monte Carlo methods, because they were less computationally intensive. With advances in computing speed, almost all simulations are now done with the Discrete Element Method (DEM). The DEM simulations integrate the equations of motion for each particle, and therefore are more accurate than the Monte Carlo methods. An overview of the DEM method is in Chapter 2. As noted multiple times in the Literature Survey, DEM and Monte Carlo simulations have been well correlated with experimental results at the qualitative level.

Due to the multitudes of affecting parameters, the behavior of a granular system is complex. Table 1.1 shows the parameter space for the "simple" granular systems that are being studies in this thesis. Parameters without a symbol are not used with a symbol in this thesis. A full explanation of these parameters are discussed in this chapter as well as in Chapter 2.

Table 1.1 Parameter Space of Simple Tapped Granular Systems

Symbol	Parameter
d	Particle diameter
N	Number of particles in the system
	Width of the system
	Vertical boundary types
	Shape of the tap
	Direction of the tap
a	Tap acceleration
f	Tap frequency
m	Particle mass
ν_0	Initial solids fraction
μ	Coefficient of friction
k	Particle stiffness
e	Restitution coefficient

1.2 Literature Survey

The sections on continuous vibration and tapping focus on the early research on granular compaction, while the section on the reversible and irreversible branch focuses on the most recent research that this thesis builds upon. The section on the boundary conditions focuses on early research with a periodic boundary condition and current research that mentions the effects of boundary conditions in granular systems.

1.2.1 Continuous Vibration

Multiple people have looked for and found the range of frequencies and amplitudes that give the densest possible result. A study by D'Appolonia and D'Appolonia in 1967 [13] tested dry sand with several amplitudes and frequencies. An extension of D'Appolonia's study by Dobry and Whitman in 1973 [14] found that the combination that gives the maximum improvement is not the combination that gives the most rapid improvement. This suggests that in a time-constrained system, such as manufacturing,

there is an optimized set of parameters that will give the most improvement in solids fraction in the least amount of time.

Experimental studies in 1951 by Stewart [15] and in 1967 by Evans and Millman [16] mapped the solids fraction after a large number of taps to the amplitude and frequency field. They found that large amplitudes combined with large frequencies resulted in a low solids fraction. The best solids fraction was found using high frequency and low amplitude, or low frequency and high amplitude. Their results pointed towards the dimensionless acceleration parameter Γ shown in Equation (1.1) as a parameter of interest in granular compaction. f is the frequency of the vibrtaion, a is the displacement amplitude, and g is the gravitational constant.

$$\Gamma = \frac{4\pi^2 f^2 a}{g} \tag{1.1}$$

A study by Zhang and Rosato in 2006 [17] studied a wide range of frequencies and amplitudes to find the pairs that would give the most improvement in the solids fraction. [17] used both DEM simulations and an experiment with acrylic monodisperse spheres in a cylinder. The system was vibrated for 10 minutes, and the change in solids fraction was measured. The results from the DEM simulations and the experiments were correlated and found to qualitatively agree.

Several early studies looked at the solids fraction of a polydisperse system vs. the time spent vibrating it. Shatalova et al. [9] looked at compacting metal powders typically used in powder metallurgy. [9] looked at many parameters to the compactions, with many experiments and values from other papers. McGeary [18] did a smaller study on a polydisperse systems of steel shot. Both [9] and [18] showed a sharp rise in solids fraction at the beginning of vibration followed by a tapering off.

Some of the early granular studies were focused on the crystal structure that can be formed by vibrating a bed of spheres. Since the highest possible solids fraction

can only be achieved with a crystalline structure, these studies are closely related to the maximum solids fraction. Berg, et al. in 1969 [19] looked at the crystal formations in an experimental three-dimensional system with both one-dimensional and three-dimensional continuous vibration. A system of ball bearings was vibrated and then frozen in water. As the ice thawed, the researchers were able to see the crystalline structure of the system. [19] found that the three-dimensional vibration gave a regular crystalline structure, while the one-dimensional vibration resulted in a disordered structure. Rocke in 1971 [20] looked at the crystal structure in a cylinder with a specially formed floor. The floor was shaped to produce cylindrical layers of hexagonal crystals. [20] then calculated a theoretical infinite-bed solids fraction and found a good match with extrapolated experimental values.

Due to the extremely complex nature of a vibrated granular system, the explanation of the phenomena behind compaction is nowhere near complete. In 1967, D'Appolonia et al. [13] attempted to explain the results of their compaction experiments. A 1994 study by Duran [21] focused on 2-dimensional systems, where the particle positions could be directly observed. The results from [20] showed that two-dimensional systems contain many of the same phenomena as 3-dimensional systems, such as convection, heaping, and size segregation [21]. Duran used aluminum beads between two glass plates and tracked the system that started from a high density state and had the solids fraction decrease as it was tapped. The conclusion in [20] is that the walls are the starting point for the decompaction, and the disorder propagated through the system from the walls.

Edwards and Oakeshott in 1989 [22] used statistical mechanics to look at a general powder that has minimal interparticle forces. They drew an analogy to thermodynamics, using the density as the temperature of the system. Follow up work on statistical mechanics in a powder system was done by Mehta and Edwards in 1990 [23] and by Oakeshott and Edwards in 1992 [24].

1.2.2 Tapping

When vibrating a granular system, there are multiple phenomena occurring which affect the density of the system and its state. The system can enter a second or higher mode, with waves on the surface of the system. Allowing a system to come to a rest between taps stops the higher order modes and certain other phenomena from occurring in the granular system and makes it easier to study the remaining phenomena. A tapped system and a continuously vibrated system display similar reactions to stimulation, but due to the missing phenomena, tapped systems are a separate field of study.

In 1993, Barker and Mehta [25] did Monte Carlo simulations with monodisperse, frictionless spheres. Their Monte Carlo model was based on a dilation and redeposition based partially on random events and partially on mechanics. The system was roughly 8 sphere diameters wide and 20 sphere diameters tall, with periodic boundaries. They plotted the density with respect to the number of taps for a range of intensities, and found that the density of the system decreased with increasing intensity. A plain exponential function was not sufficient, but a sum of two exponential functions best described the data. They theorized that there could be two different phenomena responsible for the densification process: the short-time-scale relaxation is due to the reorganization of individual particles, and the long-time-scale relaxation is due to the reorganization of clusters of particles. The formation of arches and bridges was observed in their systems, and larger arches were observed in the systems with higher intensity tapping.

Hong et al. in 1994 [26] proposed a continuum model based on diffusing voids. The model proposed by Hong et al. predicts a power-law dependence of the change in solids fraction $\Delta\nu$ to the number of taps t with Equation (1.2).

$$\Delta\nu(t) \propto t^{-2} \tag{1.2}$$

In 1995, Knight et al. [27] experimentally studied the density of a monodisperse granular system under discrete taps as it progressed from its initial state to an equilibrium state, getting quantitatively similar results to McGeary [18], who used a polydisperse system under continuous vibration. The system for [27] was glass beads in a Pyrex cylinder, with the cylinder 9.4 particle diameters wide. The initial height of the system was roughly 43.5 particle diameters deep. Knight et al. attempted various fits to their data. The sum of two exponentials proposed in [25] was found to be close, but not conclusive. A stretched exponential, also known as the Kohlrausch-Williams-Watts (KWW) function, fit well. The power law function proposed in [26] did not fit well. They observed that the relaxation looked logarithmic, and a logarithmic decay function seen in Equation (1.3) had a better fit than the stretched exponential function. The logarithmic decay was not theoretically motivated. t is the tap number, $\nu(t)$ is the density after t taps, ν_∞ is the final density, ν_0 is the initial density, and β and τ are constants.

$$\nu(t) = \nu_\infty - \frac{\nu_0 - \nu_\infty}{1 + \beta \ln\left(1 + \frac{t}{\tau}\right)} \tag{1.3}$$

Linz [28] followed up on [27] in 1996 by using a phenomenological decay law to model the densification curve. The model was based on the stroboscopic decay law, with the result shown in Equation (1.4). It was shown in [28] that Equation (1.4) matched Equation (1.3) within a first order approximation. Ψ is the digamma function, and C and D are constants.

$$\nu(t) = \nu_\infty + \frac{\nu_0 - \nu_\infty}{1 + CD\left[\Psi(t + 1 + D) - \Psi(1 + D)\right]} \tag{1.4}$$

Nowak et al. in 1998 [29] followed up on [27] by doing more studies with Monte Carlo simulations. They proposed a new model for density relaxation based on the

parking lot model. The presumption is that the denser a system is, the harder it is to pack one more particle into the same space. The Monte Carlo simulations were run with the parking lot model. The parking lot model was able to simulate the rapid rise in density followed by a slow rise. However, the parking lot model used in [29] was not able to model the steady-state fluctuations that were seen in the experimental data.

In 2005, Ribière et al. [30] used experiments with large systems of beads and rice to look at convection in a tapped system. They found the convection to present in areas that were not compacted to a dense state. The simulations started at a loose state and immediately started tapping at the final velocity. [30] also had Monte Carlo simulations with 4096 particles to take a general look at tapped granular systems and make qualitative comparisons with the experiments.

In follow-up work to [30], Ribière et al. focused on the grain motion during a tap [31]. They used a simulation to see the effect of disallowing "jumps" made by a particle in the Γ range where particles normally are caged by their neighbors. The simulation method did not track the forces between particles as in a DEM method, but artificially dilated the system and allowed it to come to rest without allowing any overlap. [31] found that there is a noticeable slowing of the densification process as well as a reduction in final density caused by disallowing "jumps."

1.2.3 Reversible and Irreversible Branch

When starting at a loose configuration and tapping a system, there will be a tap amplitude that will give the densest resulting configuration. The reversible branch is achieved by decreasing the amplitude of the tap in steps from that densest configuration. The density of the configuration when reducing the amplitude will stay the same or increase from the densest configuration achieved while increasing the amplitude. When starting at a high density and increasing the amplitude, the density decreases, following the curve by which it increased. Thus, the reversible branch can be reproduced while

sweeping the amplitude up and down, while the irreversible branch can only be seen once when increasing the amplitude from a loose state. The process of increasing then decreasing the amplitude is called "annealing" when drawing comparisons between granular systems and molecular dynamics.

An experimental study by Nowak et al. in 1997 [32] plotted the reversible branch for tapped granular systems. Their study used three systems of 1, 2, and 3mm glass beads in a tube 18.6mm in diameter and 1000mm high. The number of particles was roughly 250,000 for the 1mm particles, 32,000 for the 2mm particles, and 9500 for the 3mm particles. The tube was evacuated to remove the effect of air viscosity. The density was measured both by fill height and by using capacitive probes on the side of the tube. The systems were tapped with full sine waves at 30 Hz with varying amplitudes. Figure 1.2.3 shows a depiction of the reversible and irreversible branch from [32].

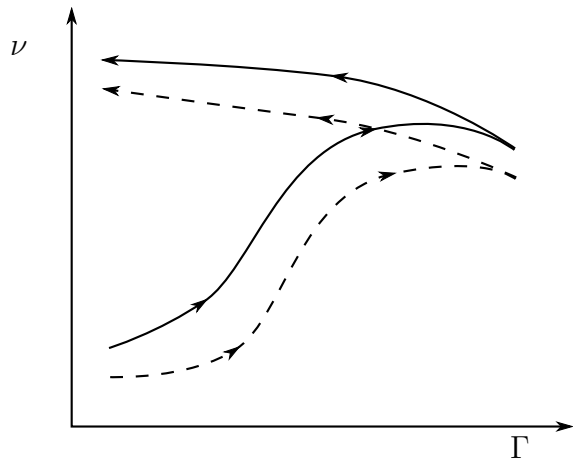

Figure 1.1 The reversible and irreversible branches of tapped granular systems. The dotted line represents 10^2 taps between data points, and the solid line represents 10^5 taps between data points.
Source: Depiction of data from [32].

The reversible branch is expected in a tapped granular system, as the understanding of granular systems is that a certain amount of energy is needed

to form or break up the microstructure. Thus, the low intensity taps are unable to form a dense microstructure, nor are the low intensity taps able to break up a dense microstructure that has already been formed.

In [32], Nowak et al. also showed the difference that the number of taps will make when sweeping the amplitudes up and down. Figure 1.2.3 shows the difference in density that additional taps has. Nowak et al. note that even after 10^5 taps, their systems may not have been run to a true steady state. Therefore, they do not know if the reversible and irreversible curves collapse to one another with a larger number of taps. However, Nowak et al. hypothesizes that the low amplitudes are being stuck in a metastable state that is less than the optimal amplitude. The system is unable to break out of the metastable states because there is no exponential tail of input energy as there is in a thermodynamic system.

1.2.4 Boundary Conditions

In physical tapping and vibration experiments, there are vertical walls that act as boundaries to contain the particles. These walls affect the system in various ways, including inducing and breaking up order in the system and relieving some of the pressure on the lower particles. In very large physical systems with small particles, such as an earthquake or a rail car full of grain, the center of the system is unaffected by the presence of the walls which are far away. However, running experiments with wide systems and many particles requires an excitation system with a higher energy capacity, which can be prohibitively expensive to acquire and run. Thus, most experiments are done with small systems where the walls effects could have an impact on the results obtained.

In a simulated system, computational time is expensive. Thus, it is prohibitively time-consuming to run large systems with many, many particles over long periods of time. In addition, a computational system with many particles requires a lot of

memory, which is expensive. In order to remove some of the effects of solid walls from the experimental results, a computational system can remove the walls and instead allow the system to "wrap around" itself. This is called a periodic boundary condition. To illustrate, consider the system in Figure 1.2.4. The striped particle, near the left boundary, is touching the shaded particles. The forces and interactions of the striped particle are passing through the boundary. If the forces in the system reorder the system and push the striped particle to the left, it will "wrap around" and come in on the right boundary, as seen in Figure 1.2.4.

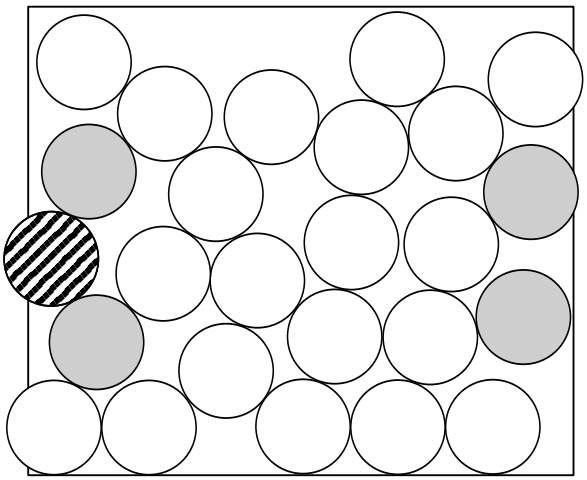

Figure 1.2 Depiction of forces transmitted through a periodic boundary. The box represents the boundary. The shaded circles represent particles that are neighbors of the striped particle, while the light particles are not neighbors of the striped particle.

The periodic boundary condition has been in use almost as long as computers have been used to simulate granular systems. Walton and Braun in 1985 [33] and Zhang and Cundall in 1986 [34] ran simulations with periodic boundaries. Their systems had a few hundred particles. Henrique et. al in 2001 [35] noted that periodic boundary conditions in a granular gas can cause the granular gas to rotate even though the initial state was irrotational. The explanation given by Henrique et. al does not apply to this thesis because the particles in this thesis come to a rest before being excited again.

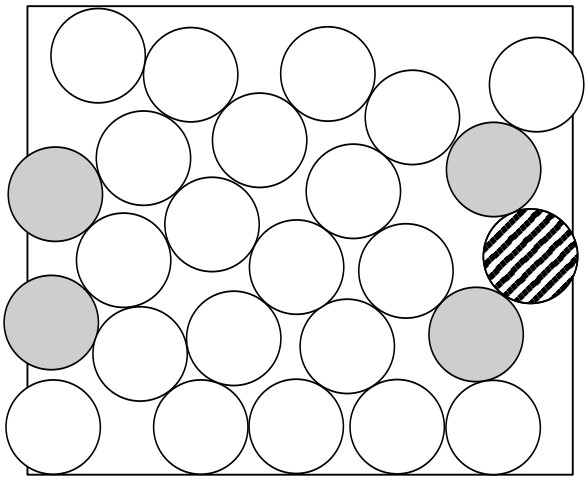

Figure 1.3 Depiction of a particle going through a periodic boundary. The box represents the boundary. The shaded circles represent particles that are neighbors of the striped particle, while the light particles are not neighbors of the striped particle.

1.3 Objective

This thesis investigates the effects of boundaries on the evolution of density in assemblies of granular particles, modeled as inelastic, frictional soft spheres, which are energized through the imposition "taps" to a supporting floor. The state of the system is characterized by the bulk solids fraction. The speed of the densification process is a key tool used to examine the differences between periodic-walled granular systems and solid-walled granular systems. The average mean squared displacement is used to investigate the boundary condition's effect on the movement of the particles during a tap.

The study will be done with DEM simulations. The modeled systems are 2cm acrylic beads in a 40cm column with a 12cm wide square base. Taps are applied as half-sine waves. The simulations use a partially elastic soft-sphere model with Hookean-spring normal forces, and a Mindlin-Deresiewicz tangential force model. The vertical boundaries are referred to as "walls" and are either periodic or solid, while the horizontal boundary is the "floor" and it is always solid.

1.4 Thesis Outline

The DEM simulation model and details are explained in Chapter 2. Ensemble of periodic-walled granular systems with a large number of taps in the irreversible region is discussed in Chapter 3. Chapter 4 is concerned with the solid vs. periodic walls study. Horizontal taps are explored in Chapter 5. Chapter 6 has a summary, conclusions, and a discussion of future work. Appendix A contains a typical input file for the DEM simulation program, and Appendix B has the code modifications required to do mean squared displacement calculations.

CHAPTER 2

OVERVIEW OF THE DISCRETE ELEMENT MODEL

2.1 Introduction

The Discrete Element Method (DEM) is a model for simulating a granular system by solving Newton's equations of motion for a system of particles that interact via soft or hard contact forces. Here, the term "hard" refers to instantaneous interactions governed by pre-collisional kinematics and particle properties. "Soft" contact forces refer to interactions that are typically functions of an allowed overlap between particles so that there is a finite duration of the contact. The equations of motion are integrated using the velocity-Verlet algorithm, and the collisions are partially elastic. This chapter explains key details of the simulations.

2.2 Force Model

Contact interactions used in this study are the soft-sphere models described in detail in [36]. The particles are spheres that are allowed to overlap, also known as the soft-sphere model. The normal contact force between the particles is linearly related with the overlap between the particles, similar to two masses attached to a linear spring. In order to model the energy loss when two particle collide, the model uses two equations for the force depending on whether the particles are moving toward or apart from each other, as seen in Equation 2.1. F_n is the normal force, k_1 is the loading spring constant, k_2 is the unloading spring constant, x is the overlap, and α is the disengagement overlap. α is defined by Equation 2.2, where x_{max} is the maximum overlap during the history of the collision.

$$F_n = \begin{cases} k_1 x & \text{moving together} \\ k_2(x-\alpha) & \text{moving apart} \end{cases} \tag{2.1}$$

$$k_1 x_{max} = k_2(x_{max} - \alpha) \implies \alpha = x_{max}\left(1 - \frac{k_1}{k_2}\right) \tag{2.2}$$

The two spring constants are related by the restitution coefficient e in Equation 2.3. k_1 is always less than k_2.

$$e = \sqrt{\frac{k_1}{k_2}} \tag{2.3}$$

The tangential force is determined by a Mindlin-Deresiewicz model, which allows for sticking as well as slipping. The tangential force is determined using Equation 2.4, where F_t is the tangential force, k_t is the tangential spring constant, and x_t is the tangential displacement between the particles.

$$F_t = k_t x_t \tag{2.4}$$

The tangential spring constant is described in Equation 2.5. $F_{t,p}$ is the tangential force during the last timestep, $F_{t,max}$ is the maximum tangential force during the history of the collision, and μ is the coefficient of static friction. The $\pm$ corresponds to decreasing/increasing F_t over the last two timesteps.

$$k_t = 0.8k_1\left[1 - \frac{\pm\left(F_{t,max} - F_{t,p}\right)}{\mu F_n \pm F_{t,max}}\right]^{1/3} \tag{2.5}$$

2.3 System Boundaries

Figure 2.3 shows the boundaries of the system. The vertical boundaries, or walls, of the system are periodic for some cases and solid in other cases. Whether the walls are periodic or solid is always specified. The floor of the system is always solid. The vertical boundaries are 12 particle diameters apart. The depth of the system is about

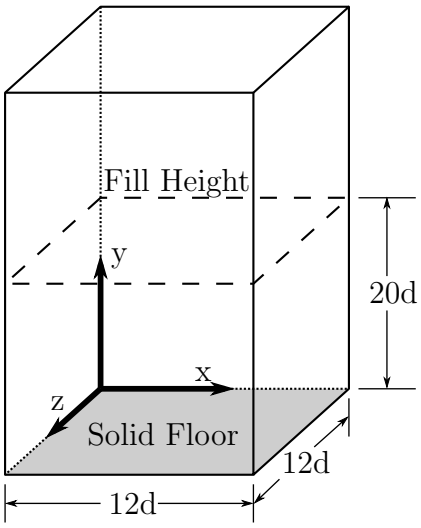

Figure 2.1 Depiction of system boundaries. The y is the vertical axis, x is across the page, and z is perpendicular to the plane of the page.

22 particle diameters before the first tap. In an ordered close packed state, the depth of the system is around 19 particle diameters.

During vertical tapping, the vertical walls of the system do not move. Since the code calculates tangential forces, the vertical walls are thus acting as a drag on the particles touching the walls during a tap. The horizontal floor follows a half-sine wave in the y direction during the excitation phase, and then is held steady during the relaxation period. The relaxation period is long enough to allow the system to come to a rest. Figure 2.3 shows a graph of the floor position vs. time during one tap. The frequencies of the taps in this thesis are all $f = 15$Hz.

During horizontal tapping, the vertical walls normal to the x direction follow the half-sine wave tap shown in Figure 2.3. The horizontal floor follows the movement of the walls in the x direction. Thus, all boundaries are moving together during a horizontal tap. All systems that are horizontally tapped have solid walls.

The particles' interactions with the boundary use the same soft-sphere force model as between two particles.

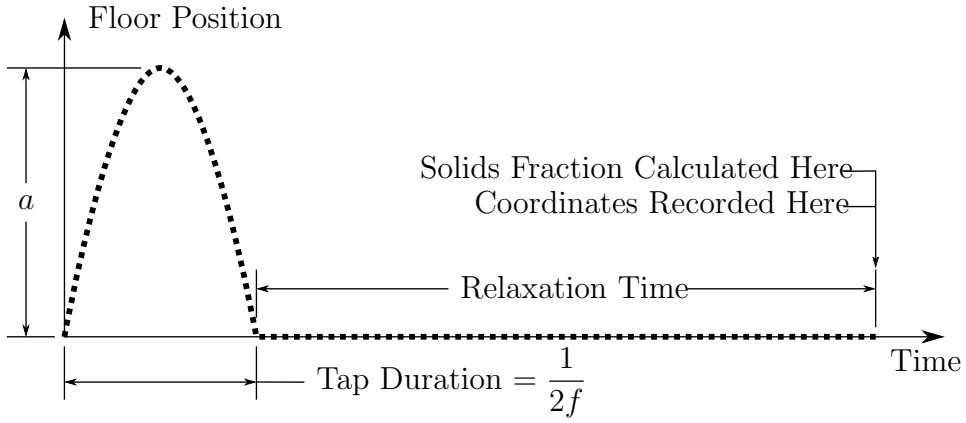

Figure 2.2 Depiction of the boundary position during a tap.

The compuational cell is the region in which the program is looking for particles to integrate. The compuational cell is the same as the system boundaries when no excitation is being applied. The system is high enough that there is never any particle near the top of the computational cell.

2.4 Near Neighbor Search

In order for the simulation program to know which particles are colliding or are going to collide, the program keeps a Verlet table of interactions between particles. The Verlet table contains interaction information for all pairs of particles within a particle radius of each other. This allows the Verlet table to be updated only when it is likely that a pair of particles not in the Verlet table is going to collide. Because updating the Verlet table is time-consuming, being able to not update the Verlet table every timestep allows the program to run faster.

Because the Verlet table is not updated every timestep, the timing of the Verlet table updates is important. The algorithm used by the simulation program sums the farthest distance moved by any single particle during a timestep. Once the sum

reaches a critical value, another Verlet table update is done and the sum reset before the next timestep is integrated.

Figure 2.4 is a demonstration of what needs to happen to update in time to catch colliding particles in the worst case scenario. Figure 2.4 shows the two fastest particles in the system, and these two particles are moving directly towards each other. In sub-figure a, and update is done. The two particles are just a trifle more than a search radius apart, so they are not counted as neighbors. Several timesteps happen between subfigures a and b. During those timesteps, the particles move the exact same distance towards each other, and that distance is a trifle less than the distance needed to trigger an update. Between sub-figures b and c, a single timestep happens. The particles have again moved towards each other, but they are still not touching. However, the sum of the distances moved for any particle is more than the trigger distance, and an update is triggered after the timestep shown in sub-figure c.

The critical question is then the question of the trigger distance. A trigger distance of half of the search radius is clearly too large since the particles could overlap before an update of the Verlet table happens. The solution used by the simulation program is to subtract the maximum distance moved by any particle from half of the search radius. This solution is not perfect, since two accelerating particles that are moving faster than any other particle, have identical velocities and accelerations, are moving directly towards each other, start only a trifle outside the search radius, and travel to only a trifle inside the trigger distance will not be caught before collision. This is because, during acceleration, the maximum distance traveled during the current timestep is less than the distance moved during the next timestep, so the overlap between the particle before they are considered neighbors will be two trifles less than twice the difference in velocities between the two timesteps. This algorithm, although flawed, is accepted because of the unlikelihood of all conditions being met at the same

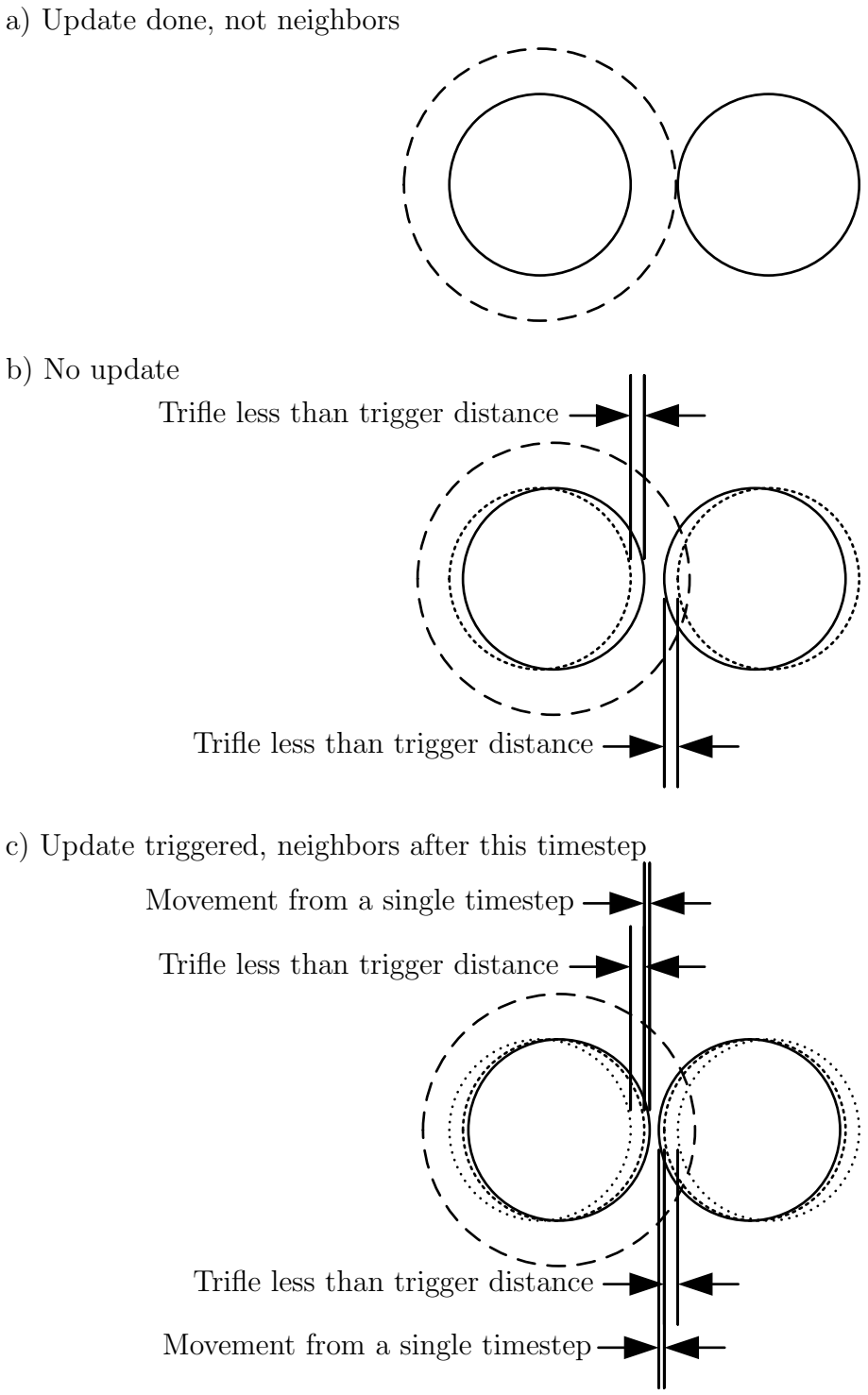

Figure 2.3 Demonstration of near neighbor searching. The large dashed circle is the near neighbor search radius. The solid circles are the current positions, the fine dashed circles are the previous positions, and the fine dotted lines are the positions two steps before.

time in a system of thousands of particles, and because the resulting error will be tiny in comparison to cumulative rounding errors that happen in the computer simulation.

The chain-cell search method allows the program to update the Verlet table more quickly at the expense of having a larger Verlet table. The chain-cell search method divides the computational cell into small cells which are slightly larger than one particle diameter in dimension. Near neighbors are all particles inside the same cell or any adjacent cell as the particle in question. Using a rapid algorithm for assigning particles to cells, this method avoids finding the inter-particle distance between all particles in the system. However, the chain-cell search algorithm is only faster for systems of 20,000 particles or more.

The chain-cell search algorithm used in the DEM simulation program for this work was done by Sweetman [37], but its potential was not realized due to the lack of computational resources necessary to run the larger systems.

2.5 Solids Fraction

The solids fraction ν is the primary method of determining the state of the system. It is the volume of a number of particles divided by the volume taken up by those particles. The solids fraction is also known as the packing density. The average solids fractions of the systems presented in this thesis are calculated using only 80% of the fill height of the system. If the fill height after a tap is 20 particle diameters, then the algorithm uses the box as $12 \times 12 \times (20 \times 0.8)$ particle diameters as the volume taken up by the particles. The volume of the particles is the sum of the volumes of all particles below $20 \times 0.8 = 16$ particle diameters in the y-axis. If a particle is only partially below 16 particle diameters, then the algorithm will slice that particle and use only the portion that is below 16 particle diameters in the y-axis.

The maximum solids fraction that can be reached by a 3D ordered system is hypothesized to be 0.74048:. per Equation 2.6 [2]. This solids fraction is attained in an Hexagonal Close Pack or Face Centered Cubic crystal structure.

$$\nu_{max} = \frac{\pi}{\sqrt{18}} \approx 0.74048 \tag{2.6}$$

The initial solids fraction of the periodic-walled systems is 0.617 with a standard deviation of 0.001. The initial solids fraction of the solid-walled systems is 0.589 with a standard deviation of 0.001.

The local solids fraction is determined using the Voronoi cell volume of each particle as the space taken by that particle. The Voronoi cell for a particle is the locus of all points closer to the particle than to any other particle. Thus, the Voronoi cell is a metric for space taken by that particle. The Voronoi graph is space-filling. Equation 2.7 shows the calculation of the local solids fraction. V_{cell} is the volume of the Voronoi cell surrounding the particle i.

$$\nu_{local}(i) = \frac{V_{particle}}{V_{cell}} = \frac{\frac{\pi d^2}{3}}{V_{cell}} \tag{2.7}$$

Figure 2.5 shows the local solids fraction distribution of a poured granular system. Sub-figure a shows the initial state of the system, immediately after pouring. The mean of sub-figure a is 0.618 and the standard deviation is 0.031. Sub-figure b shows the local solids fraction distribution of the same system after it has reached an ordered close-packed state. The mean of sub-figure b is 0.708 and the standard deviation is 0.032.

2.6 Mean Squared Displacement

The Mean Squared Displacement (MSD) is a parameter that is used to better understand the effects of the boundary conditions on the evolution of the system. The

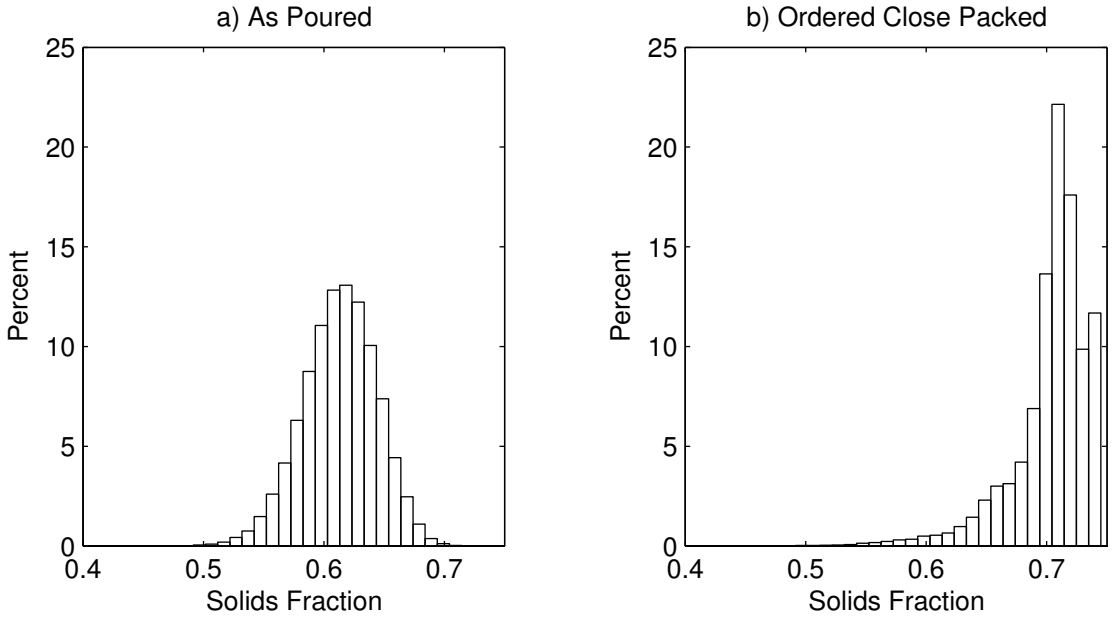

Figure 2.4 Locals solids fraction distribution of a typical system. Sub-figure a has a mean of 0.618 and a standard deviation of 0.031. Sub-figure b has a mean of 0.708 and a standard deviation of 0.032.

mean squared displacement tracks how much a particle has traveled since the tracking was begun. Equation 2.8 shows the mean squared displacement. n_{ts} is the number of timesteps since the tracking began. N is the number of particles, and x is the position of the particle in the x-direction.

$$MSD_x(t) = \left\langle |x|^2 \right\rangle (t) = \sum_{i=1}^{n_{ts}} \frac{1}{N} \sum_{j=1}^{N} \left[x_j(t_i) - x_j(t_{i-1}) \right]^2 \tag{2.8}$$

Dividing the mean squared displacement by the number of taps during the tracking time represents the relative amount of movement a particle experiences during a tap. Equation 2.9 shows the mean squared displacement per tap. n_{taps} is the number of taps since the tracking began.

$$\frac{MSD_x}{tap} = \frac{1}{n_{taps}} \sum_{i=1}^{n_{ts}} \frac{1}{N} \sum_{j=1}^{N} \left[x_j(t_i) - x_j(t_{i-1}) \right]^2 \tag{2.9}$$

Appendix A contains the changes to the source code of the program required to implement mean squared displacement calculations.

2.7 Ensemble Averaging

This thesis makes use of ensembles of systems. The individual cases in the ensemble are given the exact same tapping regimen. The only difference between the cases is that the initial pour has different random positions. The initial state of the system is statistically similar concerning solids fraction.

Because the exact densification path that a system follows is dependent on the microstructure of the system, different systems that are statistically similar will have different densification paths. Ensemble averaging is done to remove the effects of the randomness in the pour, providing an average densification path.

2.8 Values of System Parameters

The simulations in this thesis use 3456 acrylic spheres of diameter 0.02 meters. The gravitational acceleration is $g = 9.81\text{m/s}^2$ and the frequency is $f = 15\text{Hz}$. The restitution coefficient is 0.9, and the particle density is 1200 kg/m^3.

The timestep is based on the period of the loading spring. Equation 2.10 shows how the timestep is calculated. Δt is the timestep length, m is the mass of a particle, and p is the number of timesteps per collision. Previous work has indicated that values of p between 40 and 60 are reasonable [38]. For $\Gamma = 3$ with $p = 40$, this works out to be around 6.3×10^{-6}.

$$\Delta t = \frac{\pi e \sqrt{\frac{m}{2k_1}}}{p} \tag{2.10}$$

Appendix B contains a sample input file for the DEM simulation program along with an explanation for select input file parameters.

CHAPTER 3

RELAXATION CASE STUDIES

3.1 Introduction

The relaxation case studies are investigating the long term tapping on an ensemble of 25 periodic-walled systems. The original purpose of the relaxation case studies described herein was to model the reversible/irreversible phenomenology observed in experiments [32], but to start with a system that has already been relaxed at an Γ below the Γ where the peak density occurs. The expectation is that the systems will rise a little, but not rise all the way to the reversible branch.

An ensemble of 25 systems are run for 600 to 650 taps at $\Gamma = 3$. Figure 3.1 shows the evolution of the solids fraction for those taps at $\Gamma = 3$. For comparison, Figure 3.1 shows the ensemble average of the 25 systems after tapping at different intensities for 650 taps. The last taps from the 25 systems are then copied and used as the initial coordinates for 2 ensembles of 25 systems. One ensemble is tapped at $\Gamma = 2.75$, and the other ensemble is tapped at $\Gamma = 3.25$.

3.2 Results

The two ensembles are tapped for at least 6000 taps after being started. The systems did not reach a steady state value even after 6000 taps. Thus, the original goal of running multiple ensembles at reducing intensities could not be completed.

Figure 3.2a shows the solids fraction of all of the $\Gamma = 3$ taps and the subsequent taps as $\Gamma = 3.25$. Several systems reached a mostly ordered state with a solids fraction around 0.7. Several of those systems first reached a metastable state, with a solids fraction around 0.67, then continued to densify.

Figure 3.2b shows the solids fraction of all of the $\Gamma = 3$ taps and the subsequent taps at $\Gamma = 2.75$. One of the systems relaxed to a mostly ordered state, with a solids

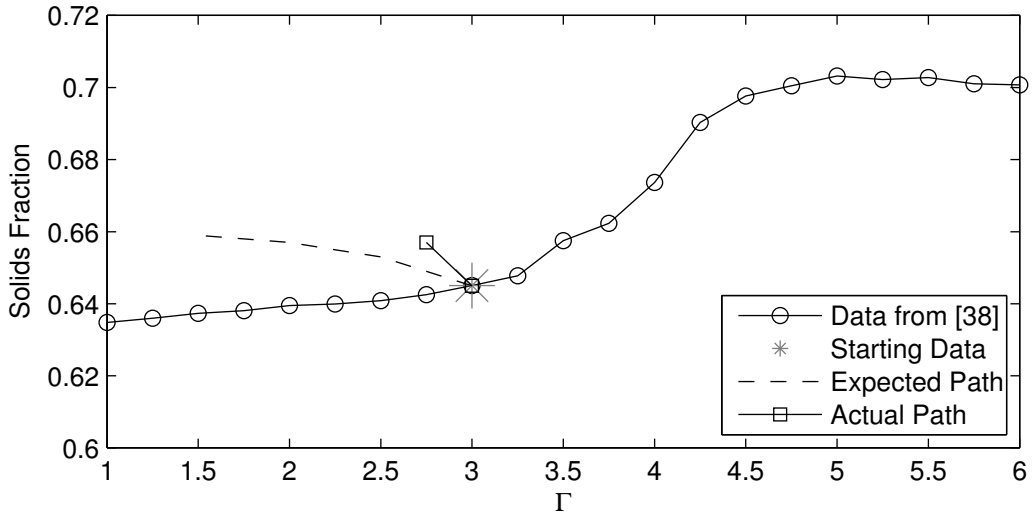

Figure 3.1 Solids fraction of ensembles as a function of tap intensity after 650 taps. The star represents the ensemble used as a basis for the ensembles in this chapter. The dashed line is the expectation for the data generated from the relaxation case studies, while the square markers represent the actual data gathered.
Source: [39]

fraction of 0.70. Many systems came to the minimum random close packed state with a solids fraction around 0.64. Several systems came to an intermediate metastable state with a solids fraction around 0.66 to 0.68.

Figure 3.2 shows the average solids fraction from Figure 3.2. There are a lesser number of taps shown in Figure 3.2 than in Figure 3.2 because not all systems were run to the same number of taps, and the average is only valid when all systems are taken into account. Even though the $\Gamma = 3.25$ systems were not given as many taps as the $\Gamma = 2.75$ systems, the $\Gamma = 3.25$ ensemble average has risen much higher than the $\Gamma = 2.75$ ensemble average. This is because there are more $\Gamma = 3.25$ systems settling to a ordered close packed state.

Figure 3.2 shows realization 18 tapped at $\Gamma = 3.25$ after 2300 taps. The bulk solids fraction is around 0.65, but the local solids fraction varies widely from the maximum of 0.74 at the bottom to 0.58 in the middle. The dark blue particles at the

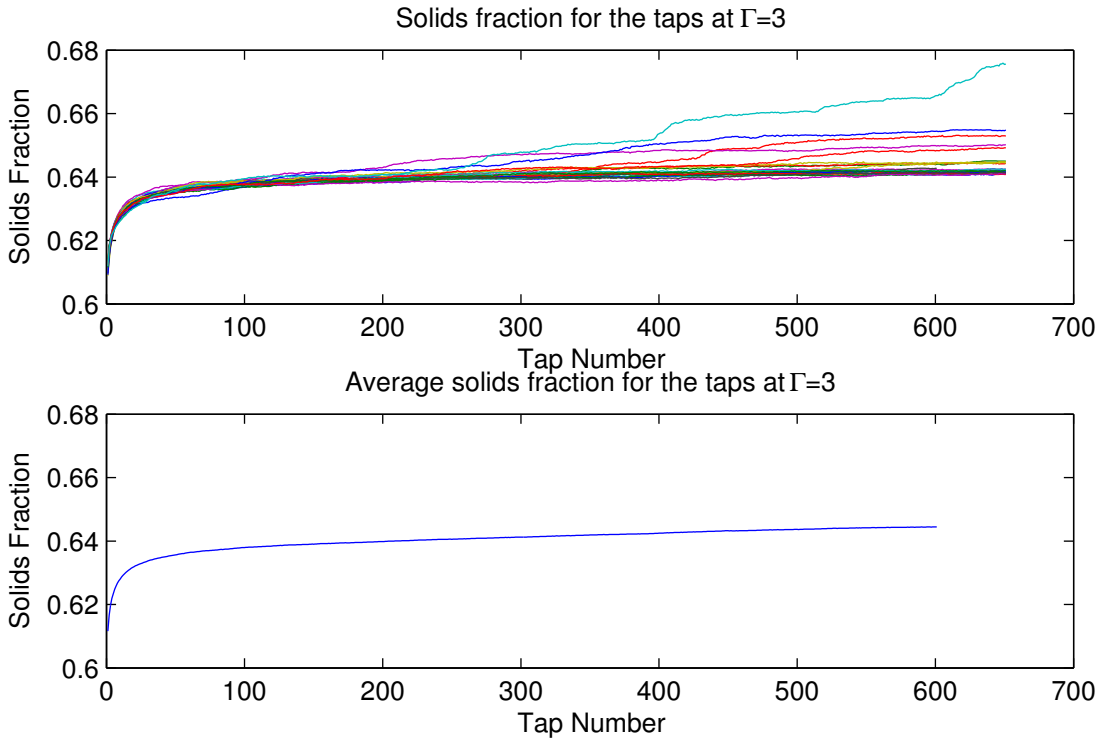

Figure 3.2 Solids fraction of the ensemble run at $\Gamma = 3$. Sub-figure a) shows the solids fraction of every realization, while sub-figure b) shows the ensemble average solids fraction.
Source: [39]

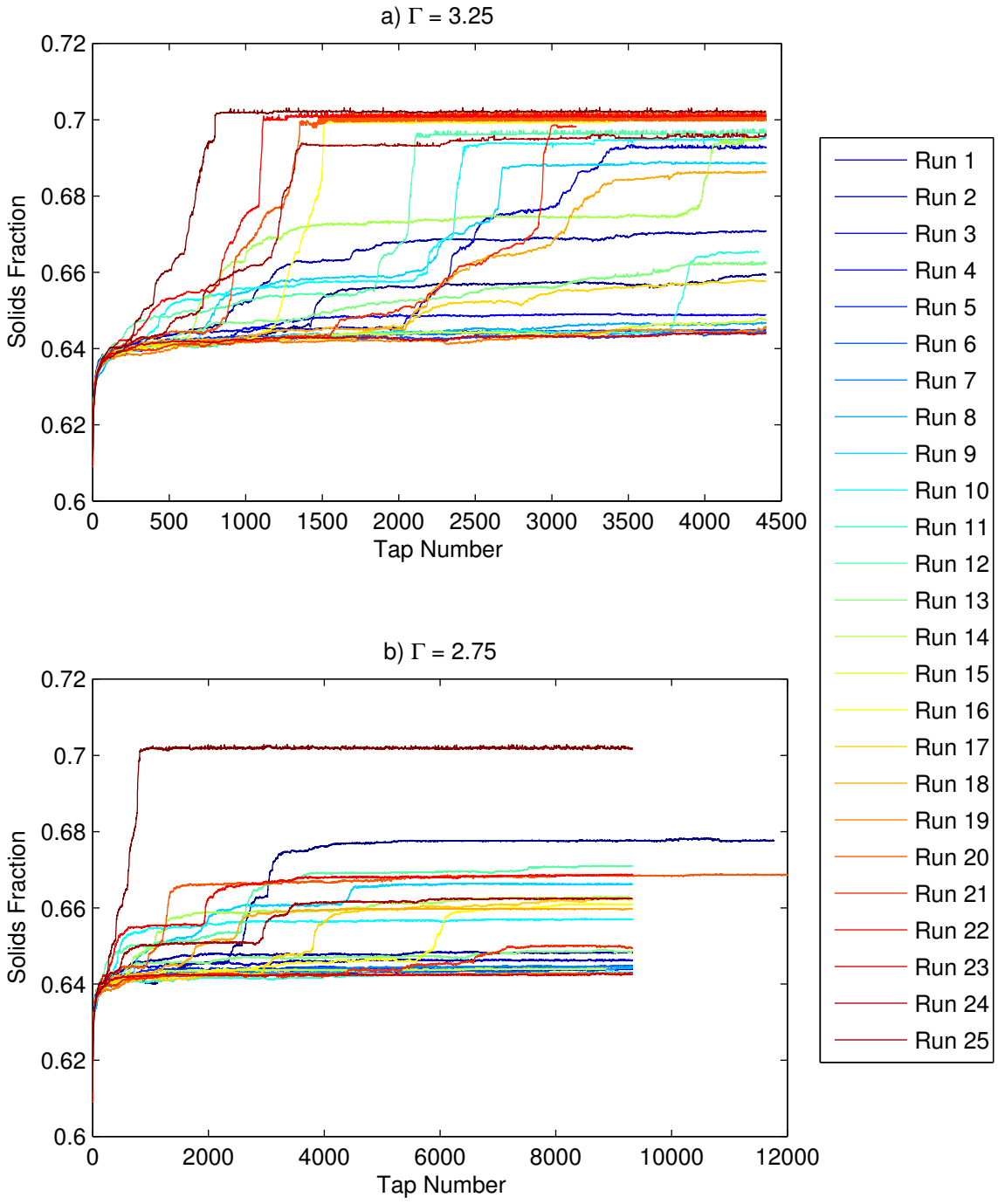

Figure 3.3 Solids fraction of systems.

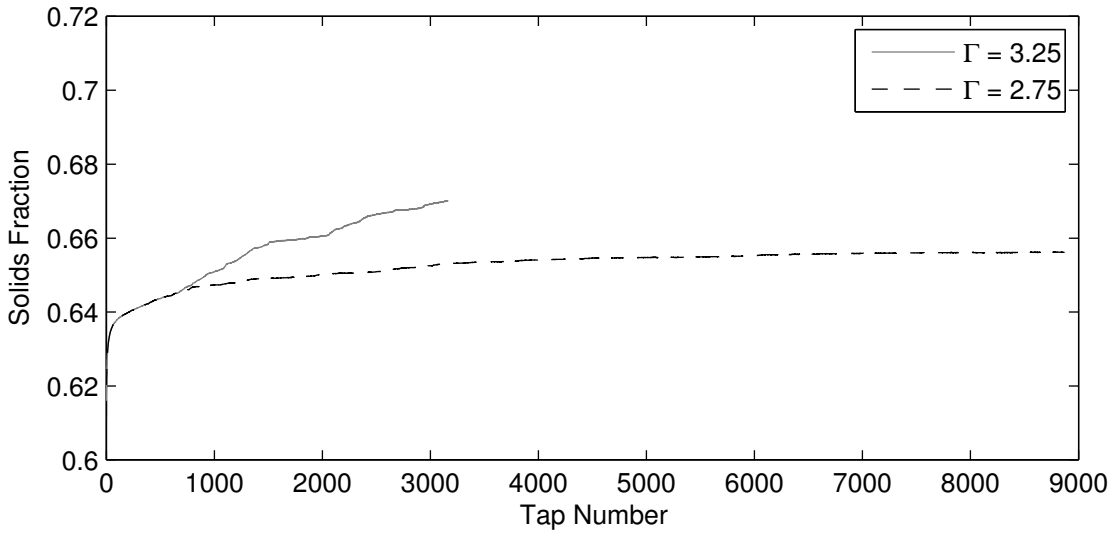

Figure 3.4 Ensemble average of solids fractions of systems.

top of the realization do not have an accurate Voronoi cell volume because they have no neighboring particles above them.

A continuous bulk movement is observed in several realizations. Figure 3.2 shows the y-z positions of the particles in realization 18 tapped at $\Gamma = 3.25$ after tap 3500. Figure 3.2 can be likened to X-ray images of the realization showing only the particle centers. Figures 3.2, 3.2, and 3.2 show the positions of the particles after tap 3502, 3504, and 3506, respectively. The microstructure is similar between all of the figures, but the position of the particles steadily shifts to the right between each figure.

Figure 3.2 shows the solids fraction of realization 18 tapped at $\Gamma = 3.25$. The system is in a metastable state around tap 3500.

The bulk movement can also be seen by the movement of individual particles. Figure 3.2 shows the position of particle 10 in realization 18 tapped at $\Gamma = 3.25$. Particle 10 is near the top of the system, close to but not part of the free surface. Sub-figures a through c show the movement of the particle in the x, y, and z directions, respectively. The movement of the particle in the x direction is similar for each tap, but after the tap, the particle comes to a rest in a different position than when it

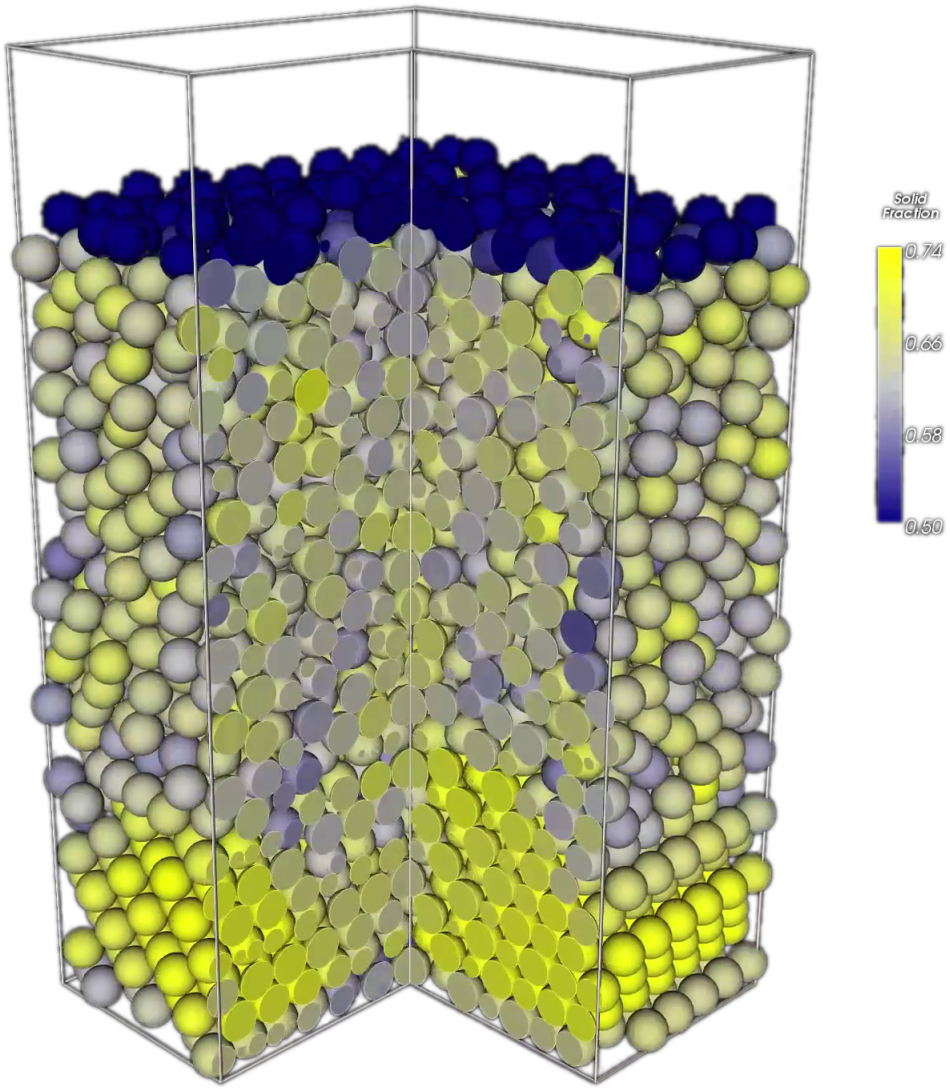

Figure 3.5 Realization 18 tapped at $\Gamma = 3.25$ after 2300 taps. Yellow represents high-density areas where the local solids fraction is 0.74. Blue represents low-density areas where the solids fraction is 0.5.

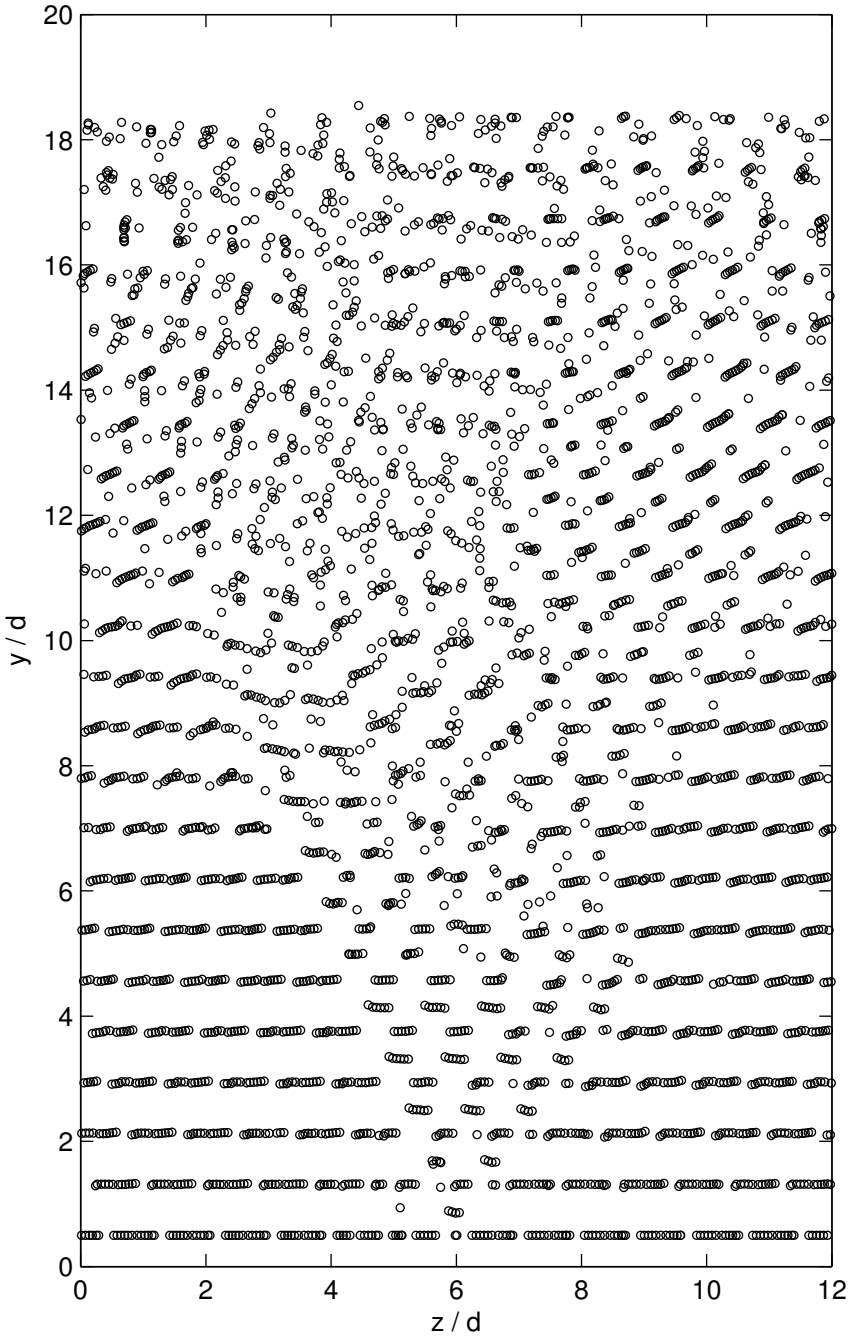

Figure 3.6 The y-z positions of the particles in realization 18 tapped at $\Gamma = 3$ after tap 3500.

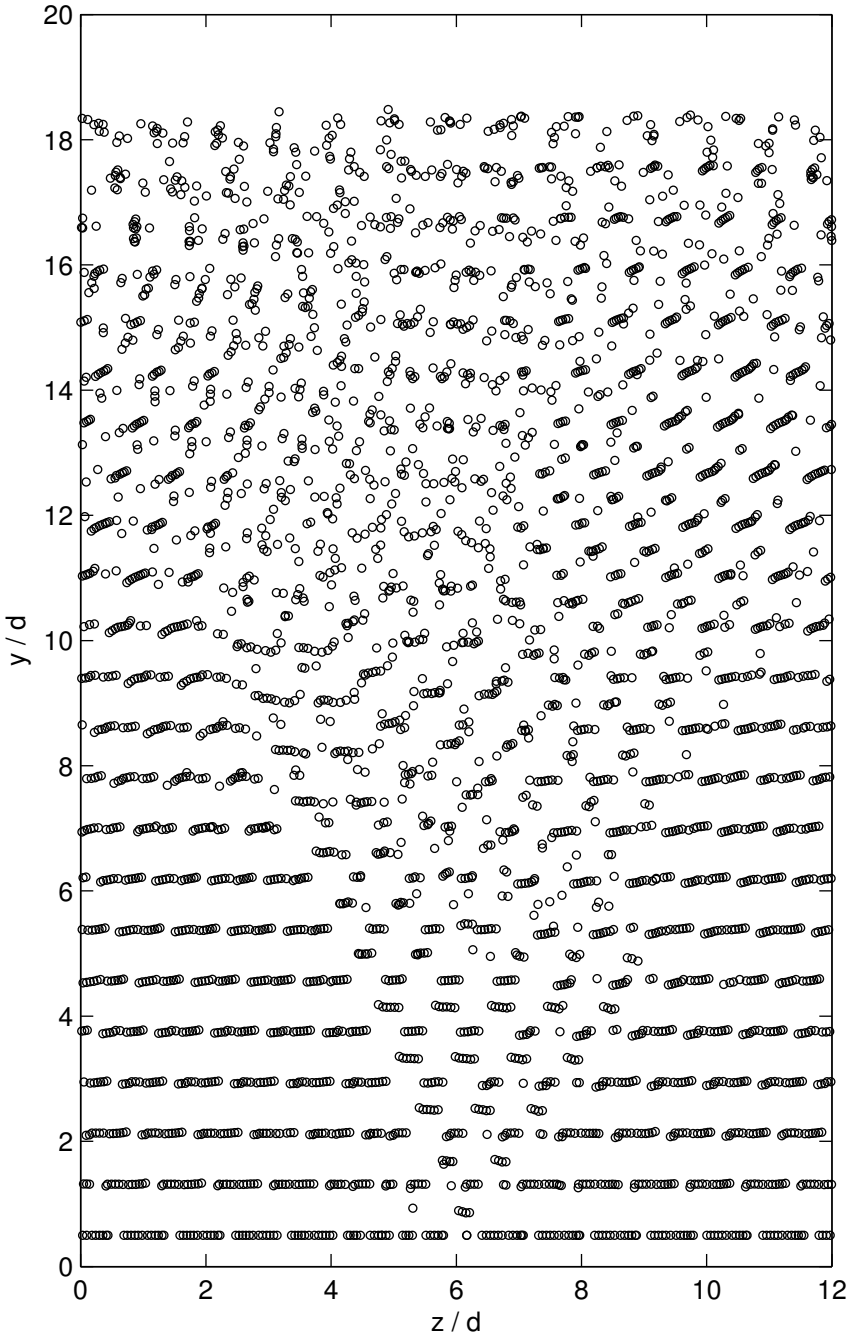

Figure 3.7 The y-z positions of the particles in realization 18 tapped at $\Gamma = 3$ after tap 3502.

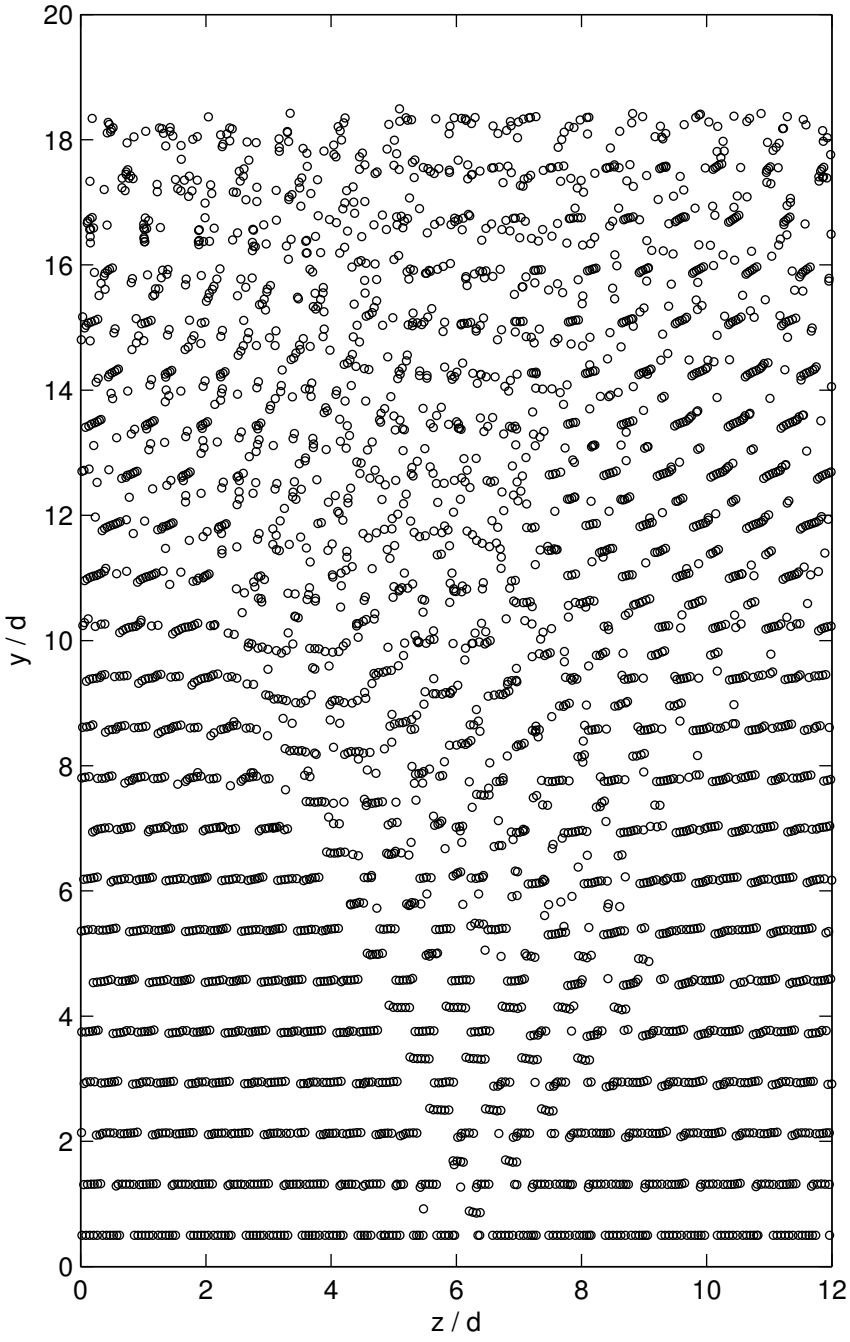

Figure 3.8 The y-z positions of the particles in realization 18 tapped at $\Gamma = 3$ after tap 3504.

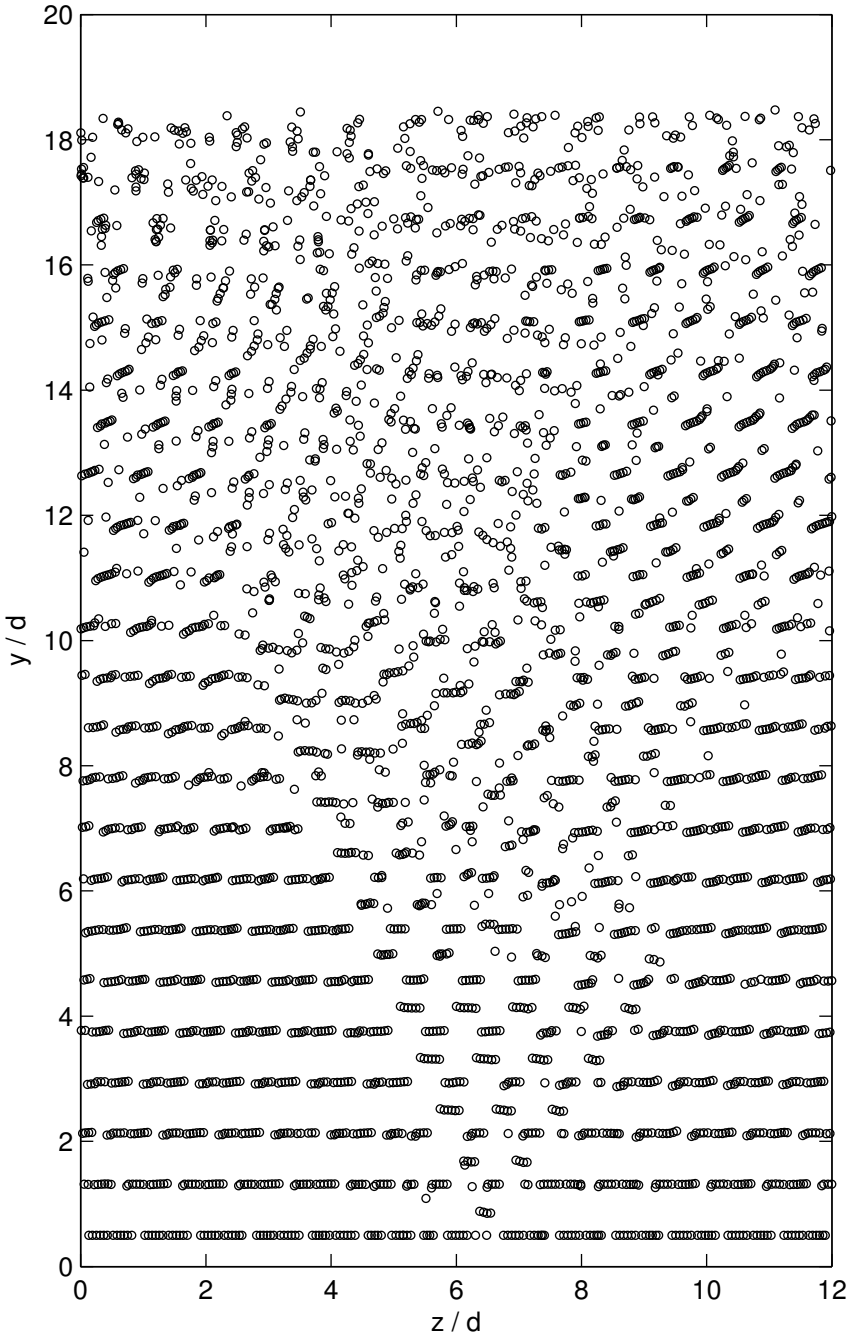

Figure 3.9 The y-z positions of the particles in realization 18 tapped at $\Gamma = 3$ after tap 3506.

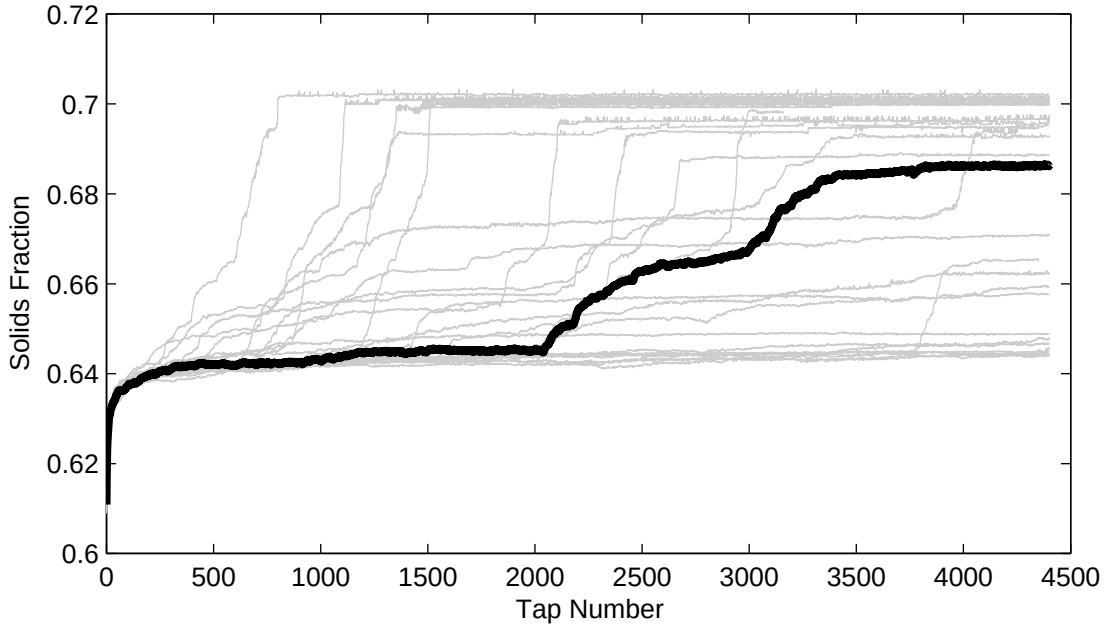

Figure 3.10 Solids fraction of realization 18 at $\Gamma = 3.25$.

started. The bulk movement of the particle in the z direction is even more than the movement of the particle in the x direction. The z direction also displays more variation in the movement during a tap.

Because the systems are tapped, all momentums in the system should be zero before every tap. The relaxation time is confirmed to be sufficient to allow the system to come to a rest before the next tap. Figure 3.2 shows the position of particle 10 in realization 18 tapped at $\Gamma = 3.25$. The position does differ, but the average slopes of the lines remain the same. The difference is due to accumulated numerical error.

The bulk movement was observed in several other realizations. Equation 3.1 gives a value of the bulk movement averaged over 100 taps, where T is the tap number and N is the number of particles. Figure 3.2 shows the average bulk movement during the last 100 taps of each realization. A realization that has high movement at $\Gamma = 3.25$ has low movement in a different direction at $\Gamma = 2.75$. Therefore, there does

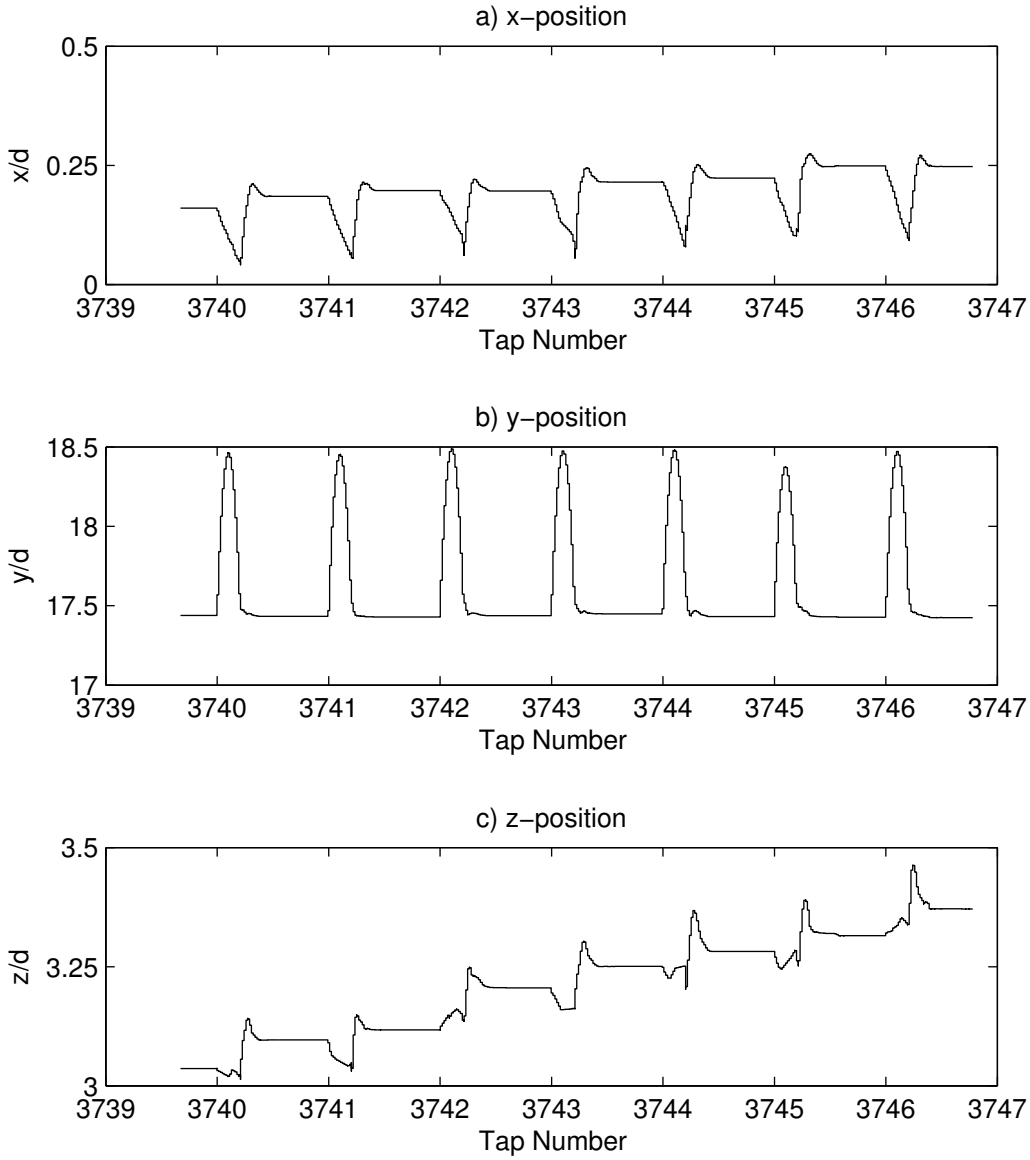

Figure 3.11 The position of particle 10 in realization 18 tapped at $\Gamma = 3.25$.

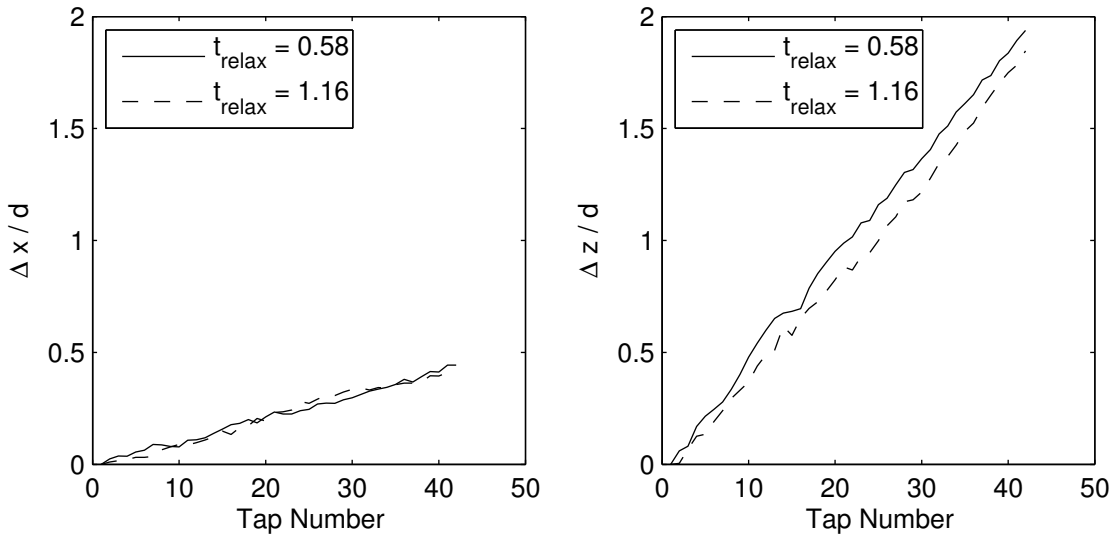

Figure 3.12 The position of particle 10 in realization 18 tapped at $\Gamma = 3.25$. The solid line is the change in position of particle 10 with the original relaxation time, and the dashed line is the change in position of particle 10 with doubled relaxation time.

not appear to be a correlation between the bulk movement in the $\Gamma = 3.25$ and the $\Gamma = 2.75$ ensembles.

$$\frac{\text{Bulk Movement}}{\text{tap}} = \frac{1}{N}\sum_{i=1}^{N}\Big[(x_i(T) - x_i(T-100))^2 + (y_i(T) - y_i(T-100))^2 + (z_i(T) - z_i(T-100))^2\Big]^{1/2} \tag{3.1}$$

A possible explanation of the bulk movement is that there is some arrangement of particles that is leaning on itself through the periodic wall. When tapped, some layers move horizontally. The horizontal movement is arrested by the tangential friction with the floor, and the system is now moved to one side slightly.

An alternative explanation for the bulk movement is that this is the result of accumulated numerical error. While this is possible, the magnitude and consistency

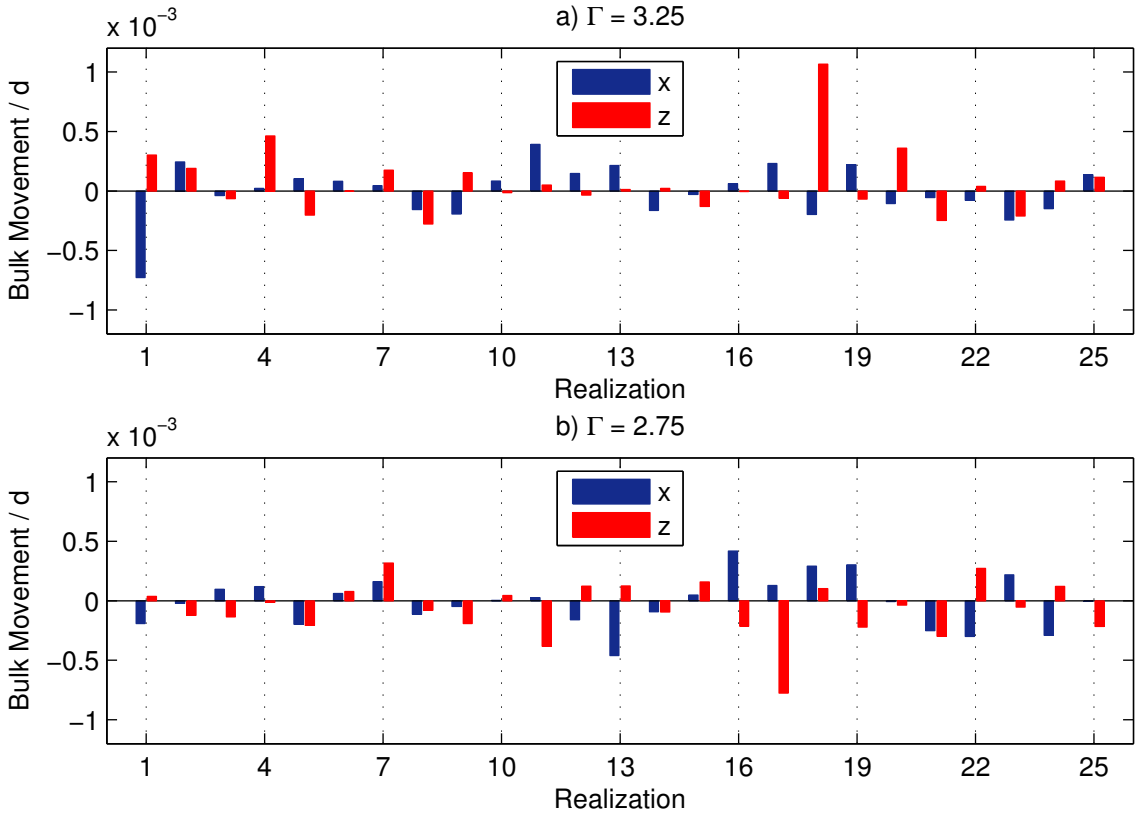

Figure 3.13 The bulk movement per tap of the systems, averaged over the last 100 taps.

of the movement indicates that this may not be the realization. Further studies may be warranted.

The $\Gamma = 3.25$ ensemble has more bulk movement than the $\Gamma = 2.75$ ensemble. There are multiple possible explanations for this phenomenon. One explanation is that the systems with a higher solids fraction have more bulk movement. Figure 3.2 shows the final solids fraction of a system vs. the average bulk movement over the last 10 taps for that system. The abscissa is represented by $(\sqrt{\Delta x^2 + \Delta z^2}/10)/d$, where the Δ is the difference between the last and the tenth-to-last tap. Figure 3.2 shows that there is no correlation between bulk movement and solids fraction.

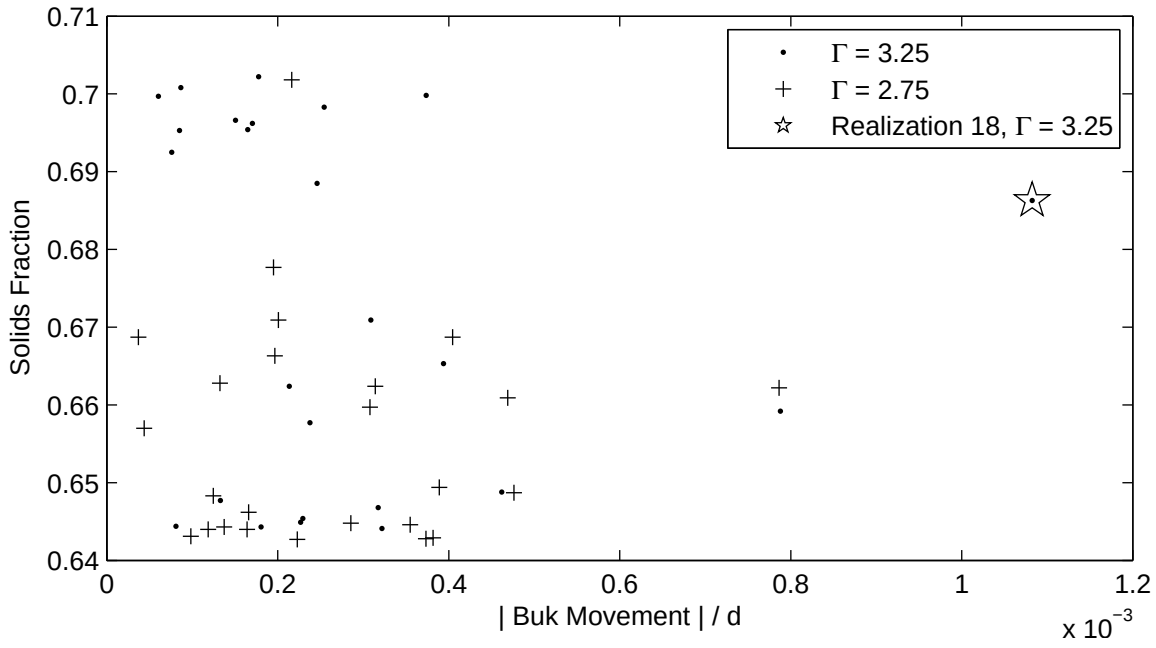

Figure 3.14 The final solids fraction vs. the average bulk movement over the last 10 taps.

Another explanation is that the $\Gamma = 3.25$ taps add more energy to the system, thus causing more bulk movement. This hypothesis is difficult to prove or disprove without knowing the exact mechanism of the bulk movement.

There are two distinct scales of crystalline formation observed. Local scale densification happens when single particles accrete on a large ordered region. Local scale densification is represented by a gradual rise in the solids fraction, or gentle acceleration of the densification rate. Large scale densification is where two or more separate ordered regions form, with a disjoint between them, and that disjoint is is rapidly removed and only one ordered region is formed. Large scale densification is represented by a sharp rise in the solids fraction over the course of 1-4 taps.

Figure 3.2 shows large scale densification happening in 2 taps. There is a large area of yellow and green particles in the circle on the left that are partially organized. In the circle on the right, the yellow and green particles have dropped into the larger crystal.

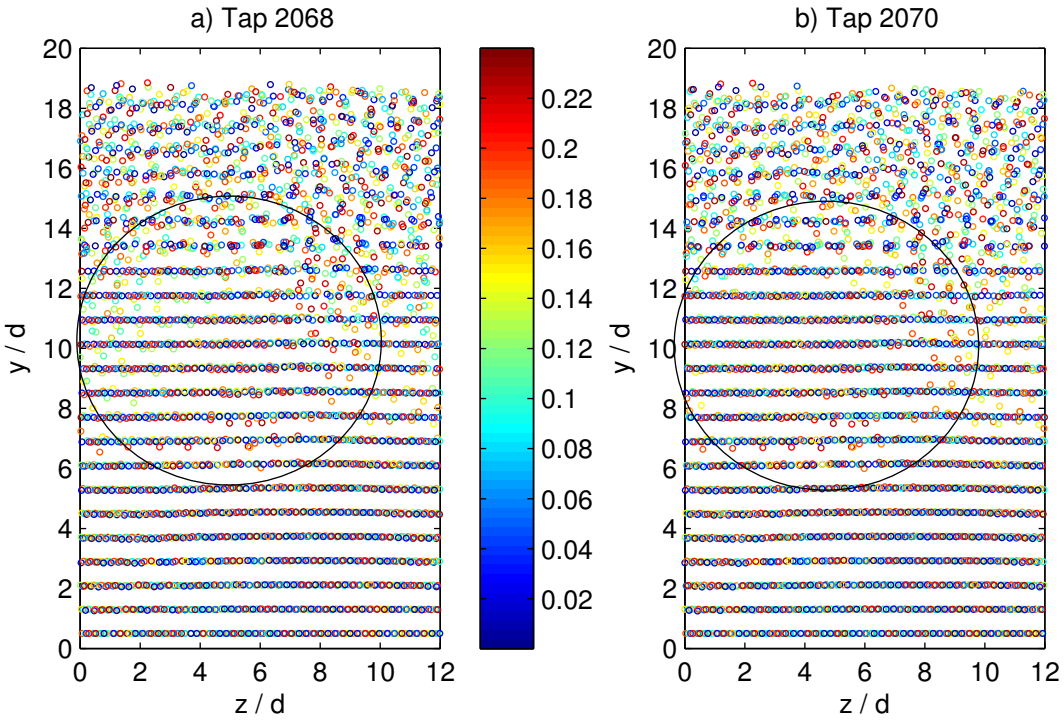

Figure 3.15 Comparison image showing large scale densification in realization 12 tapped at $\Gamma = 3.25$. Compare the yellow and green particles in the circled regions. The color of the particle shows x/d, according to the colorbar.

CHAPTER 4

SOLID VS. PERIODIC WALLS

4.1 Introduction

The solid vs. periodic wall case studies highlight the differences between systems with solid walls and systems with periodic walls to elucidate the wall effects of both periodic walls and solid walls. Three ensembles of five systems are created. One ensemble has periodic walls. Two ensembles have solid walls. One of the solid-walled ensembles has the walls stationary during the tap and is labeled "Solid Walls," and the other solid-walled ensemble has the walls moving as if they are connected to the floor and is labeled "Solid Moving Walls." Both solid wall setups reflect possible experimental setups. All three ensembles are tapped at $\Gamma = 3$.

The motivation for the solid vs. periodic wall studies is that a continuous bulk motion between taps is observed in the relaxation case studies. This behavior clearly can only occur in periodic-walled systems, where particles can exit one side and enter the other. In a solid-walled system, the solid walls would only allow the particles to gather toward one side of the system, but not allow a continuous bulk movement. This was an inspiration to investigate other effects of periodic walls.

4.2 Results

Figure 4.2 shows the solids fraction of the studied systems. The systems have reached a random close packed state, and any densification is happening slowly. No systems have jumped to an ordered close-packed state, but some systems are still slowly rising. The solid moving wall simulations were started later, and thus do not have as many taps as the other two simulations.

Figure 4.2 shows the average solids fraction for the periodic- and solid-walled systems. The solid-walled systems took longer to reach the random close packed

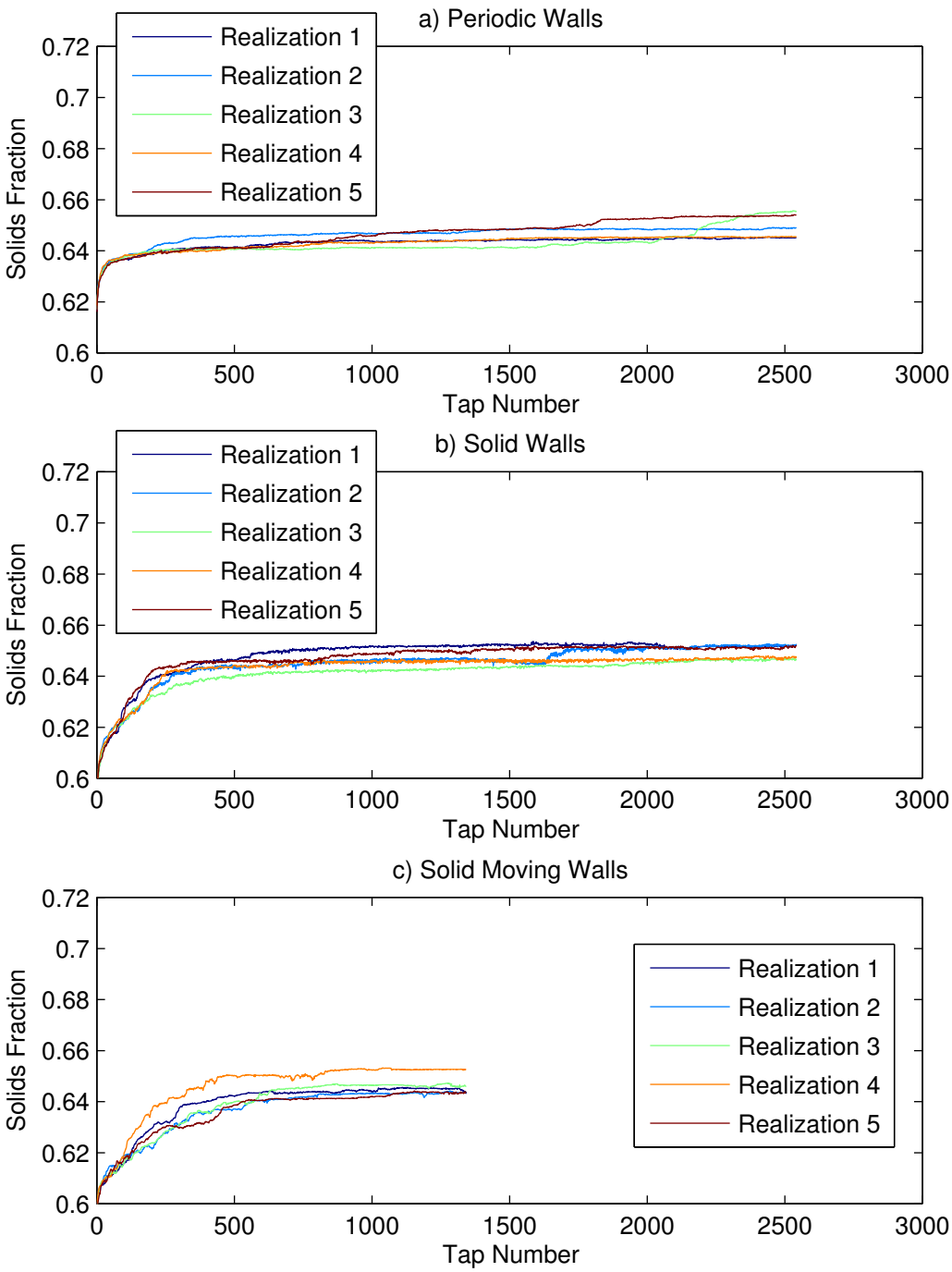

Figure 4.1 The solids fraction of a) the systems with periodic walls, b) the systems with solid stationary walls, and c) the systems with solid moving walls as a function of the tap number.

state, and are at a slightly higher density than the periodic-walled systems. The solid-moving-walled systems take an even longer time to reach the random close packed state.

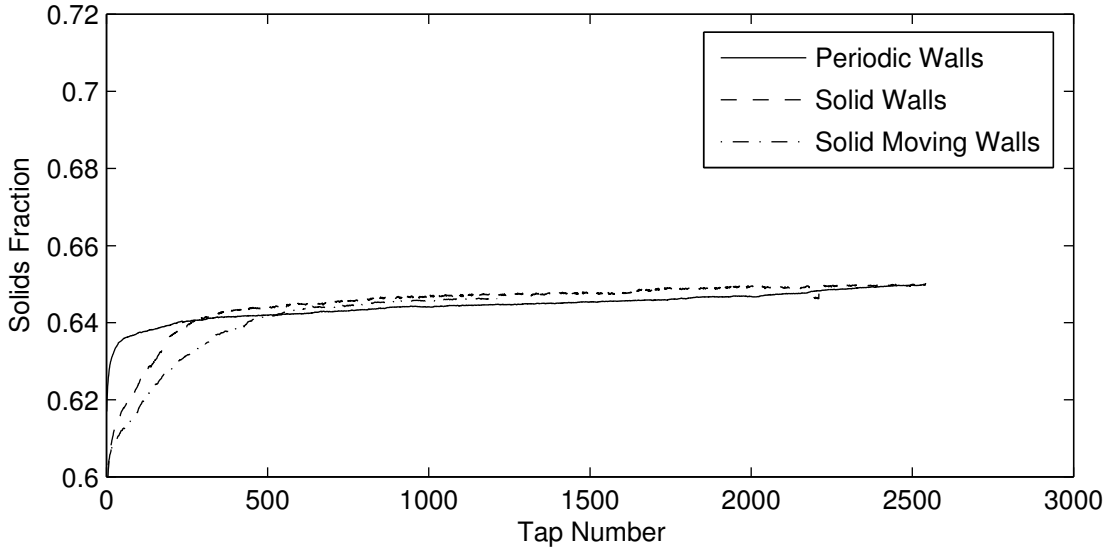

Figure 4.2 Ensemble average solids fraction for the periodic- and solid-walled systems as a function of the tap number.

An inspection of Figure 4.2 reveals that the longer initial rise of the solid-walled systems is a behavior that all of the systems exhibited. Further tapping with larger ensembles need to be done to determine if the difference in final density is due to random behavior or whether this is a wall effect.

Figure 4.2 shows the mean squared displacement in realization 1 of the periodic- and solid-walled systems. The horizontal MSD, shown in sub-figures a and c, is roughly the same for the periodic- and solid-walled systems. The vertical MSD, seen in sub-figure b, is much higher for the periodic-walled system than for the solid-walled system. The overall MSD, shown in sub-figure d, closely follows the vertical MSD because the vertical MSD is over a magnitude larger than the horizontal MSD.

Table 4.2 shows the ensemble averaged mean square displacements per tap. The vertical MSD of the solid walls is clearly less than the vertical MSD of the periodic

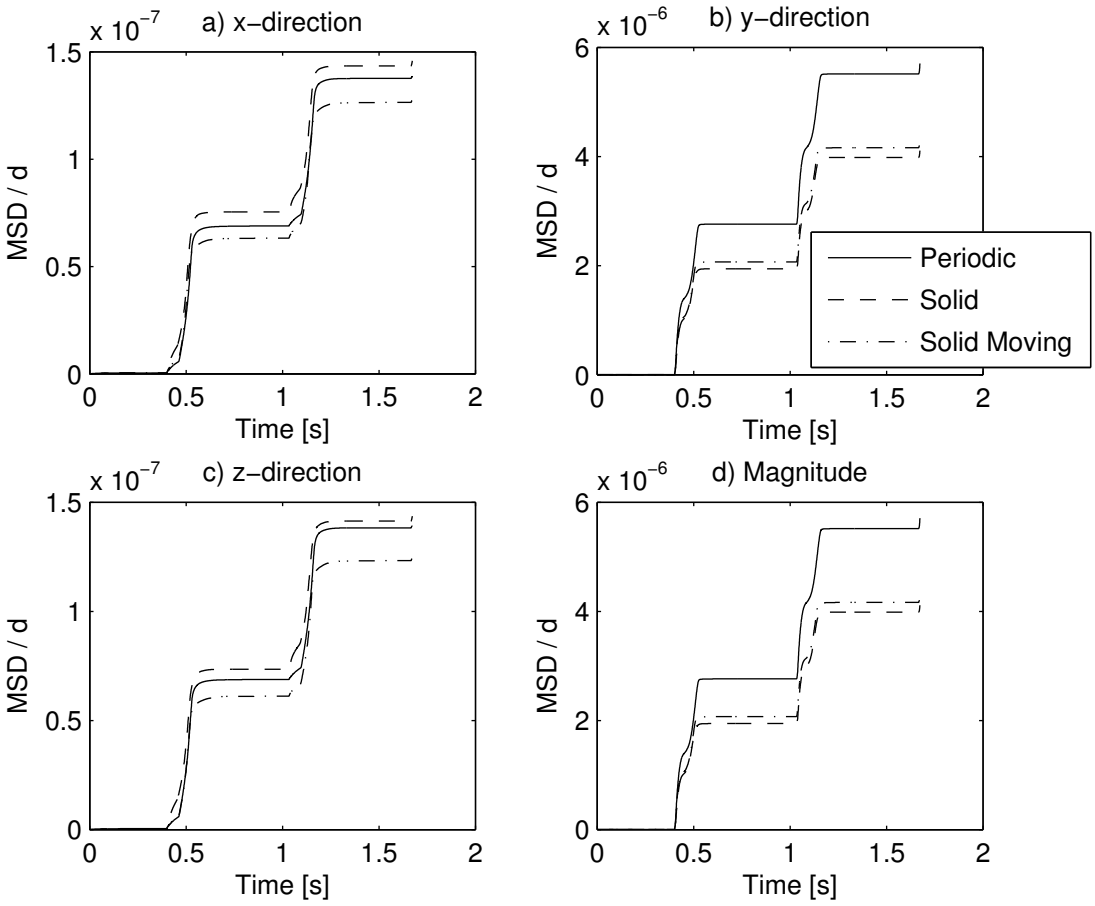

Figure 4.3 Realization average mean squared displacement for 2 taps for periodic- and solid-walled systems. Realization 1 is used as an example in both ensembles. The taps shown are taps 2526 and 2527.

walls. It is hypothesized that the solid walls are retarding the upwards motion of the realization during the tap.

Table 4.1 Mean Squared Displacement for Solid vs. Periodic Case Studies

			Ensemble average of Mean Squared Displacement per tap $\times 10^7/d$			
Intensity	Direction	Walls	x	y	z	total
$\Gamma = 3$	Vertical	Periodic	0.66	26.58	0.68	26.60
$\Gamma = 3$	Vertical	Solid	0.69	19.86	0.70	19.88
$\Gamma = 3$	Vertical	Solid Moving	0.65	19.72	0.65	19.74

CHAPTER 5

HORIZONTAL VS. VERTICAL TAPPING

5.1 Introduction

The motivation for the horizontal tapping investigation comes from both the bulk movement in the relaxation case studies and from the solid vs. periodic wall studies. The purpose of the horizontal tapping is to investigate the effect of horizontal excitation.

During a vertical tap, only the floor moves. During a horizontal tap, the walls and the floor move together. All systems are given taps at $\Gamma = 3$. Horizontal taps have the same amplitude as the vertical taps, thus the same amount of energy in imparted into the system during a horizontal tap as during a vertical tap. Five systems are given only vertical taps, i.e. in the y direction. Five systems are given only horizontal taps in the x direction. Five systems are given alternating taps in the y and the x direction. For the systems that are given alternating taps, the total number of taps is the sum of the horizontal and vertical taps. For example, an alternating system that is given 100 taps was given 50 vertical taps and 50 horizontal taps.

5.2 Results

The solids fractions of the systems are shown in Figure 5.2. All systems are behaving similarly; no system is stalling in a metastable state and then continuing to densify.

The average solids fraction of all of the systems is shown in Figure 5.2. The systems that were tapped only with vertical taps have a solids fraction similar to the solids fractions for solid-walled systems in Figure 4.2. The systems that were given alternating taps have a solids fraction slightly higher than the systems that were only given vertical taps. This behavior could be due to random effects because the systems under vertical tapping have the same solids fraction as the alternating-tapped systems

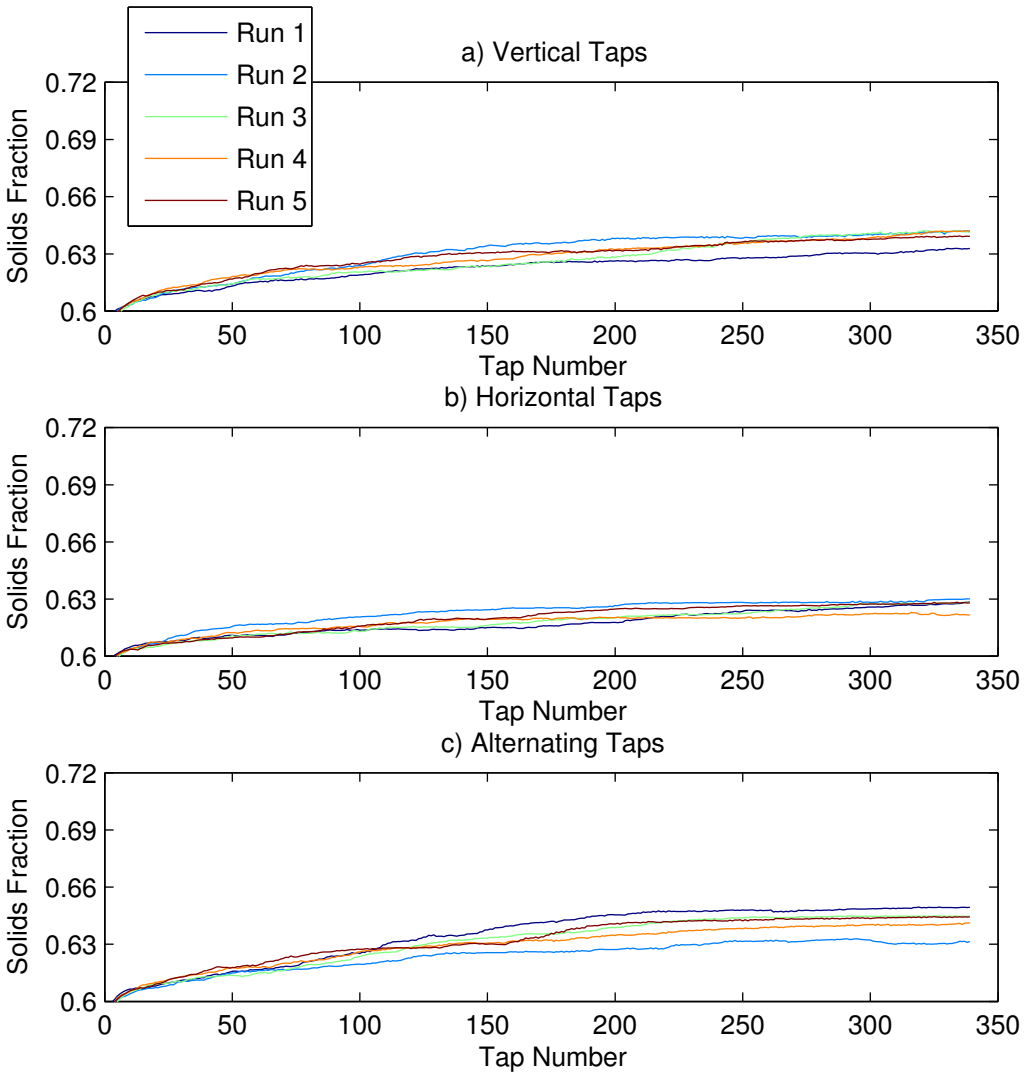

Figure 5.1 Solids fraction of systems with a) vertical taps, b) horizontal taps, and c) alternating horizontal and vertical taps.

around tap number 60, but then the solids fraction of the two ensembles diverges again.

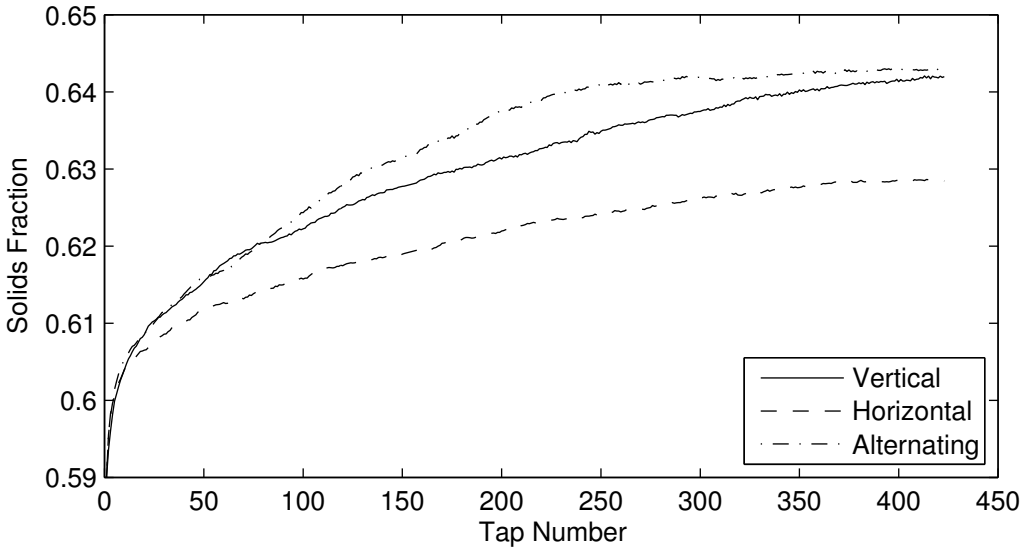

Figure 5.2 Ensemble average of the solids fraction of systems with vertical, horizontal, and alternating taps.

Figure 5.2 shows the mean squared displacement for 4 taps of realization 1, which is representative of all realizations. The x and y directions show the alternating taps as larger jumps and smaller jumps.

Table 5.2 shows the average mean squared displacement per tap for the last 10 taps and the standard deviation of the average over the ensembles. Note that alternating taps, which has a mean squared displacement as fast or faster than the vertical taps, has 38% less total mean squared displacement. The x direction MSD of the horizontal taps is much less than the y direction MSD of the vertical taps. This brings the total MSD of the horizontal taps much lower than the total MSD of either the vertical or the alternating taps.

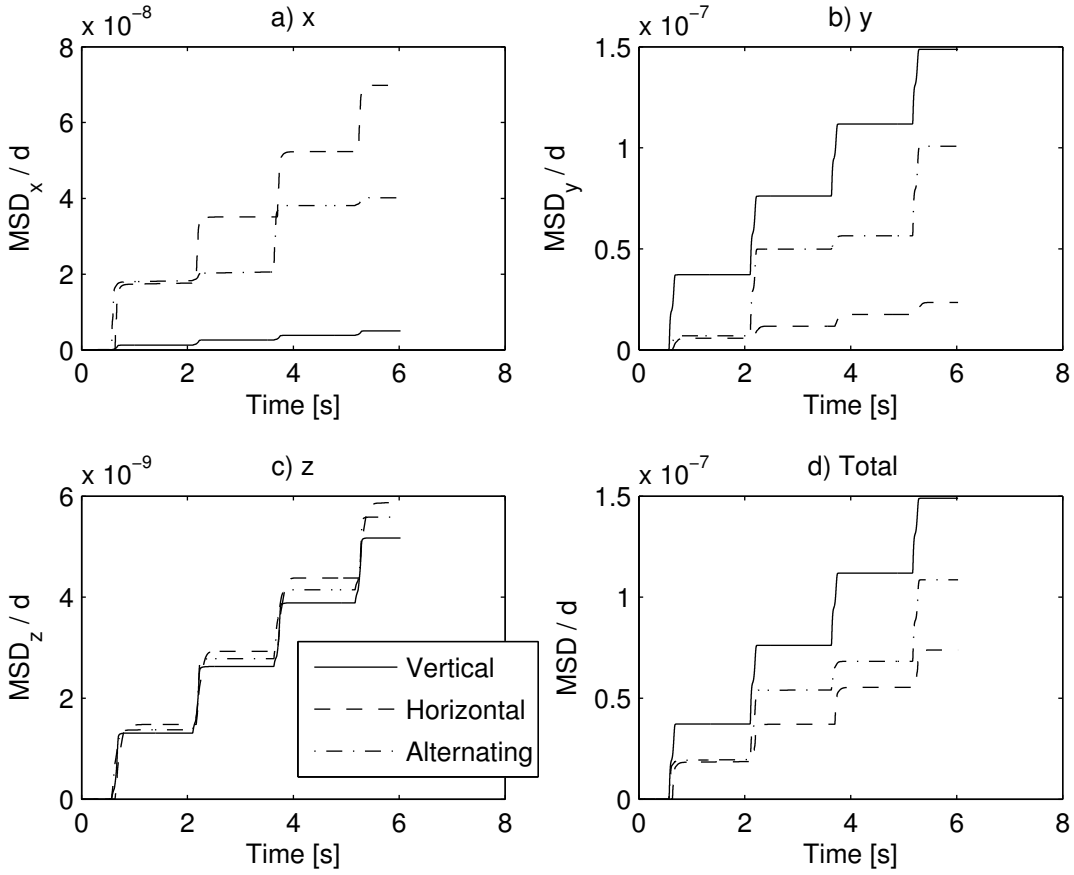

Figure 5.3 The mean squared displacement for alternating taps a) in the x direction, b) in the y direction, c) in the z direction, and d) total mean squared displacement. Note the three different orders of magnitude in the ordinates.

Table 5.1 Mean Squared Displacement for Horizontal vs. Vertical Case Studies

			Ensemble average of Mean Squared Displacement per tap $\times 10^7/d$			
Intensity	Direction	Walls	x	y	z	total
$\Gamma = 3$	Vertical	Solid	0.69	19.72	0.66	19.74
$\Gamma = 3$	Horizontal	Solid	8.51	3.18	0.68	9.11
$\Gamma = 3$	Alternating	Solid	5.49	10.70	0.67	12.18

CHAPTER 6

CONCLUSIONS AND FUTURE WORK

6.1 Summary

Chapter 3 investigates density relaxation with periodic walls. The necessity of thousands of taps is shown. The bulk movement is found and partially analyzed. Two scales of densification are discussed.

Chapter 4 delves into the effects of the walls. Periodic boundary conditions and two types of solid boundary conditions are compared with the density evolution. The mean squared displacement is used to analyze the differences.

Chapter 5 examines the solid walls in more detail using horizontal taps. Vertical, horizontal, and alternating vertical-horizontal taps are applied. The density evolution is again used to compare the boundary conditions, and the mean squared displacement offers some insight.

6.2 Observations

The relaxation case studies show that the solids fraction can temporarily halt as the system enters a metastable state. The system can leave the metastable state and continue to densify. Reaching a temporary steady state is not enough to predict whether a realization will continue to densify after more taps. The length of time that a tapped system stays in the metastable state varies, but the higher intensity taps generally results in shorter periods of time in the metastable states.

When looking at videos of cross-sections similar to Figure 3.2, it is observed that there are two scales of densification, a local-scale densification and a large-scale densification. Local scale densification happens when individual particles accrete on a large ordered region, and large scale densification happens when multiple ordered regions combine.

A notable observation from the relaxation case studies is that there can be a bulk movement in periodic-walled systems, but a cause for the bulk movement was not determined. It is noted that the higher tap intensity generally produces more bulk movement, but there is no correlation between bulk movement and solids fraction.

6.3 Conclusions

Compare the periodic walls from solid vs periodic with the alternating taps. Figure 6.3 shows the ensemble with alternating taps from Chapter 5 on the same graph as the solids fraction of the ensemble with the periodic walls from Chapter 4. The periodic-walled ensemble has reached a solids fraction of 0.636 in 50 taps, while the alternating-taps ensemble takes 4 times as long, or 200 taps, to reach a solids fraction of 0.636. In 200 taps, the alternating-taps ensemble has had 100 vertical taps. Therefore, the

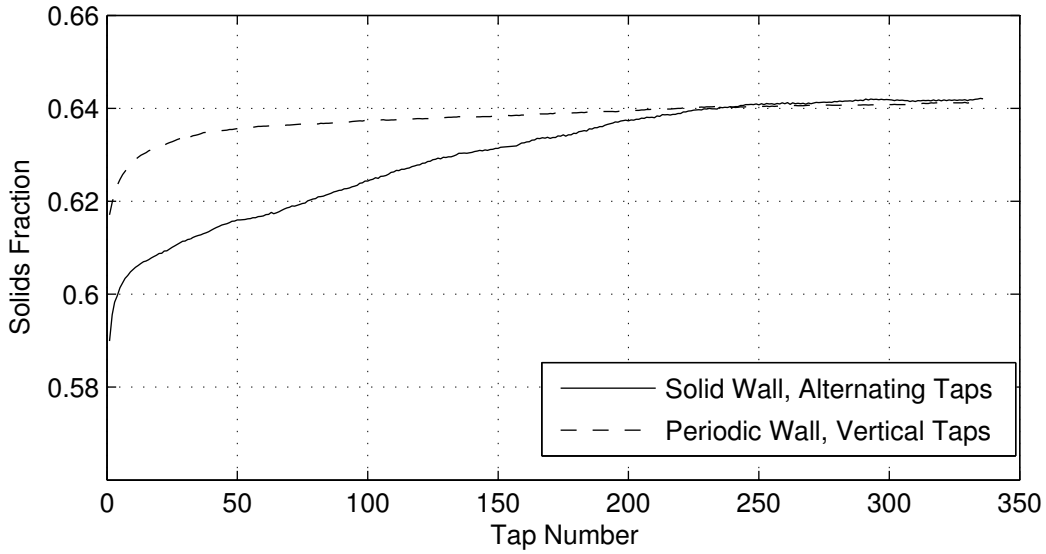

Figure 6.1 Comparison of the ensemble with periodic walls and vertical taps from Chapter 4 against the ensemble of solid walls and alternating taps from Chapter 5. $\Gamma = 3$ for both ensembles.

The periodic walls allow the densification process to happen more quickly. The conflict between the ordered regions originating from the floor and the ordered regions originating from the walls is hypothesized to slow down the densification process and interfere with the system's ability to reach an ordered close packed state.

The vertical movement of the walls during a vertical tap does not greatly affect the density evolution rate of the tapped system under these conditions. This may be coincidental, because only one set of conditions are comparable.

The horizontal tapping study showed that the systems subjected only to horizontal taps do not densify as fast as the systems subjected to vertical taps, but alternating horizontal and vertical taps densify as quickly or more quickly than vertical taps alone.

6.4 Future Work

All systems can be run longer to study long-term effects. As Chapter 3 shows, well over 10,000 taps may be necessary to achieve a steady-state value. Possibly 100,000 taps are necessary per [32].

The solid vs. periodic walls can be run for a range of intensities and system widths. As a system gets wider, the effect of the solid walls is expected to drop relative to the effects of the floor.

Investigating the cause of the bulk movement. It is necessary to investigate the movement of many individual particles over the duration of a tap for multiple systems, because multiple systems may have different exact causes for movement.

The horizontal-vertical alternating taps can be run with a range of intensities. Similarly, the moving vs. not moving solid walls under vertical tapping can be run for a range of frequencies and amplitudes.

APPENDIX A

MEAN SQUARED DISPLACEMENT CODE

Below is a patch file to the DEM simulation code to calculate the mean squared displacement. The code is in FORTRAN 90.

The patch format is unified diff. The lines beginning with "diff -u" and the triple plus-signs and dashes indicate which file is being edited. The double are codes indicating line numbers. The lines beginning with a single "+" are the new code being inserted. The lines beginning with a space are staying the same.

```
1  diff -u ../source.old/3dshear.f ./3dshear.f
2  --- ../source.old/3dshear.f     2013-05-15
       20:13:28.000000000 -0400
3  +++ ./3dshear.f 2013-11-05 22:03:56.000000000 -0500
4  @@ -178,6 +178,12 @@
5         mt1 =1
6         is0 = 0
7         ircg = 0
8  +c---- The following is for the mean square displacement.
       It is the cumulative
9  +c---- mean square displacement since the beginning of the
       tap.
10 +       msdsum(1) = 0.
11 +       msdsum(2) = 0.
12 +       msdsum(3) = 0.
13 +c---- End of code for mean square displacement.
14        write(24,*) rad(ind1)
15
16        DO 10000 i = 1, mp
17 diff -u ../source.old/integ2.f ./integ2.f
18 --- ../source.old/integ2.f      2012-12-23
       20:28:51.000000000 -0500
19 +++ ./integ2.f  2013-11-09 09:36:55.000000000 -0500
20 @@ -11,6 +11,14 @@
21        subroutine integ2
22        include 's3dscmm'
23        real tarray(2),etime
24 +c---- The following is for the mean square displacement.
       It is the cumulative
25 +c---- mean square displacement since the beginning of the
       tap.
```

```
26 +       real*8 msdstep(3)
27 +       msdstep(1) = 0.
28 +       msdstep(2) = 0.
29 +       msdstep(3) = 0.
30 +c---- End of code for mean square displacement.
31 +
32  c-----finish this integration step to obtain coordinates
       at end of
33  c-----current time step and estimation of velocities there
34  c
35 @@ -34,6 +42,12 @@
36         dx(i) = vhx(i)*dt
37         dy(i) = vhy(i)*dt
38         dz(i) = vhz(i)*dt
39 +c---- The following is for the mean square displacement.
       It is the cumulative
40 +c---- mean square displacement since the beginning of the
       tap.
41 +       msdstep(1) = msdstep(1) + ((dx(i)) ** 2)
42 +       msdstep(2) = msdstep(2) + ((dy(i)) ** 2)
43 +       msdstep(3) = msdstep(3) + ((dz(i)) ** 2)
44 +c---- End of code for mean square displacement.
45  c
46  c-----coordinates at end of time step
47         x(i) = x(i) + dx(i)
48 @@ -208,6 +222,16 @@
49  c-----The above part was added as part of the
       modifications-----------
50  c-----------------------------------------
51  c
52 +c---- The following is for the mean square displacement.
       It is the cumulative
53 +c---- mean square displacement since the beginning of the
       tap.
54 +       msdsum(1) = msdsum(1) + (msdstep(1) / 3456);
55 +       msdsum(2) = msdsum(2) + (msdstep(2) / 3456);
56 +       msdsum(3) = msdsum(3) + (msdstep(3) / 3456);
57 +       open(unit=81,file='zmsd',ACCESS='APPEND',status='
       unknown')
58 +       write(81,392)t,msdsum(1),msdsum(2),msdsum(3)
59 + 392   format(e14.8,3(1x,e14.8))
60 +       close(81)
61 +c---- End of code for mean square displacement.
62         close(61)
63         close(62)
64         close(63)
65 diff -u ../source.old/s3dscmm ./s3dscmm
```

```
66 --- ../source.old/s3dscmm       2013-03-24
      11:08:31.000000000 -0400
67 +++ ./s3dscmm   2013-11-05 22:05:38.000000000 -0500
68 @@ -35,6 +35,10 @@
69  c CCCI Next line added for chaining cells
70        real*8 celli,ttot,cellix,celliy,celliz
71        real maxtapvel
72 +c---- The following is for the mean square displacement.
      It is the cumulative
73 +c---- mean square displacement since the beginning of the
      tap.
74 +      real msdsum(3)
75 +c---- End of code for mean square displacement.
76
77  c
78  c     lcm linklist
79 @@ -259,6 +263,10 @@
80        common lenfp,lenchr,ilastll
81        common ndump1, nrun1, nout1, istart1
82        common inosave
83 +c---- The following is for the mean square displacement.
      It is the cumulative
84 +c---- mean square displacement since the beginning of the
      tap.
85 +      common msdsum
86 +c---- End of code for mean square displacement.
87  c
88        dimension dypxxk(myzone),dypyxk(myzone),dypzxk(
             myzone)
89       1         ,dypxyk(myzone),dypyyk(myzone),dypzyk(
            myzone)
```

APPENDIX B

SAMPLE INPUT FILE FOR THE DEM CODE

This input file is used for the $\Gamma = 2.75$ ensemble in Chapter 3. Modifications of certain parameters were used for the other ensembles. The format of the input file follows a FORTRAN 90 namelist.

`np` on line 4 is not the number of particles in the system, but the total number of simulated particles. It is the number of free particles plus the number of boundary "particles," which are used to simulate the solid boundaries.

`tpour` on line 35 is the relaxation time of the system.

`search` on line 40 is the search distance between particles in meters. It is discussed in more detail in Section 2.4.

`ycell` on line 41 is the height of the cell in meters.

`xyrat` and `zyrat` on lines 42 and 43 are the aspect ratios of the computational cell in the x and the z directions, respectively. Thus, the total width of the computational cell in the x direction is $xcell = xyrat \times ycell = 0.25 \times 0.96 = 0.24$.

`rmassz` on line 56 is the mass of a sphere with unit radius.

`number(1)` on line 68 is the number of free particles in the system, or 3456.

`elastb` on line 73 is the restitution coefficient.

The velocity amplitude `vamp` of the boundary is shown in Equation B.1. `vamp` is on line 75.

$$vamp = a2\pi f = \frac{\Gamma g}{4\pi^2 f^2} 2\pi f = \frac{\Gamma g}{2\pi f} \tag{B.1}$$

```
1 s3dsNEwb i3ds343b particles 30.00deg n=47 n/mm=.55294 drag
     =0.0 z=6.7mm
2 fmub=0.25 fmu=0.1
3
```

```
4  &var np = 3457 /Total number of particles in cell
5  &var nxby0 = 1 /No of boundary particles in x-dir. at y = 0
6  &var nzby0 = 1 /No of boundary particles in z-dir. at y = 0
7  &var nxby1 = 0 /No of boundary particles in x-dir. at ycell
8  &var bdry = 1 /flag for boundry type (1;cubic, 2;tringular)
9  &var nzby1 = 0 /No of boundary particles in z-dir. at ycell
10 &var nxbz0 = 0 /No of boundary particles in x-dir. at z = 0
11 &var nybz0 = 0 /No of boundary particles in y-dir. at z = 0
12 &var nxbz1 = 0 /No of boundary particles in x-dir. at zcell
13 &var nybz1 = 0 /No of boundary particles in y-dir. at zcell
14 &var nybx0 = 0 /No of boundary particles in y-dir. at x = 0
15 &var nzbx0 = 0 /No of boundary particles in z-dir. at x = 0
16 &var nybx1 = 0 /No of boundary particles in y-dir. at xcell
17 &var nzbx1 = 0 /No of boundary particles in z-dir. at xcell
18 &var nfix = 0 / number of fixed particles
19 &var nzcyl = 0 / number of fixed cylinders parallel to z-
      axis
20 &var nycyl = 0 / number of fixed cylinders parallel to y-
      axis
21 &var ncmax = 0 /number of collisions during entire run
22 &var nout = 0 /No. of time to print out results
23 &var nczero = 0 /number of collisions before start cum. ave
      .
24 &var ntcol = 40 /number of time steps during a collision
25 &var nvel = 20 /number of intervals for vel. distrib.
26 &var nyzone = 48 /number of y zones
27 &var mzcell = 4 /
28 &var nycell = 10 /
29 &var itervm = 1 /max iterations per time step
30 &var icoord = 0 /flag for coordinates print out
31 &var itty = 0 /flag for tty interaction
32 &var ixyz = 0 /flag to read init coords of fxd & bnd
      particles
33 &var istart = 1000 /to restart the code rename d3ds to
      d3ds1000 and set istart=1000
34 &var tmax = 4800 /max time for calculation
35 &var tpour = 0.52 /time for pouring
36 &var dt = 0. /time step
37 &var dtout = 0.5 /time interval for printing out results
38 &var dtdump = 2.0 /time interval for dumping
39 &var tzero = 0.25 /restart long-term cum. ave.
40 &var search = 0.008 /search distance for near neighbors;
      must be greater than 0
41 &var ycell = 0.96 /cell height (m)
42 &var xyrat = 0.25 /ratio used to compute xcell
43 &var zyrat = 0.25 /ratio used to compute zcell
44 &var vave = 0.0 /average deviatoric transl. velocity
```

```
45 &var vseed = 0.9 /seed for random initial particle
      velocities
46 &var vxzero = 0.0 /initial velocity in the x-direction (ave
      )
47 &var vyzero = 0.0 /initial velocity in y-direction (ave)
48 &var vzzero = 0.0 /loading stiffness K1
49 &var skn1 = 2.8e+05 /normal force coefficient
50 &var elast = 0.899999976 /coefficient of restitution
51 &var slope = 1.0e+05 /alternative parameter for unloading
52 &var ratk = 0.8 /ratio of tangential/normal stiffness
53 &var fmu = 0.1 /coefficient of friction
54 &var fmub = 0.3 /friction for boundary and fixed particles
55 &var power = 0.3333333 /tangential force exponent
56 &var rmassz = 5026 /mass of unit sphere
57 &var tstart= 0.0 /
58 &var gravx = 0.0 /acceleration of gravity in x direction
59 &var gravy = -9.81 /acceleration of gravity in y direction
60 &var gravz = 0.0 /acceleration of gravity in z direction
61 &var vxby0 = 0.0 /x velocity of real boundary at y = zero
62 &var vxby1 = 0.0 /x velocity of real boundary at y = ycell
63 &var vyby0 = 0.0 /
64 &var vyby1 = 0.0 /
65 &var t2move = 30.0 /time when the floor starts to move
66 &var vyfloor = 0.0 /velocity of the floor when moving
67 &var draddt = 50. /rate of increase of particle radii
68 &var number(1) = 3456 /number of particles in group 1
69 &var radius(1) = 0.01 /particle radii for group 1
70 &var number(2) = 1 /number of particles in group 2
71 &var radius(2) = 0.01 /radius of cylindrical boundry
72 &var skn1b = 2.8e+06 /
73 &var elastb = 0.9 /
74 &var slopeb = 1.0e+05 /
75 &var vamp = 0.2863247544 /velocity amplitude of boundary
76 &var frq = 15 /frequency of bump
77 &var tbump = 0.033333 /duration of one bump
78 &var nrcg = 10000 /number of bumps to be processed
79 &var finis = 1. /end
```

BIBLIOGRAPHY

[1] J. Kepler, *On the Six-Cornered Snowflake*. Original in Latin "De Nive Sexangula", Translated by Colin Hardie, 1966, 1611.

[2] T. C. Hales, "Cannonballs and honeycombs," *Notices of the American Mathematical Society*, vol. 47, no. 4, pp. 440–449, 2000.

[3] R. A. Bagnold, *The Physics of Blown Sand and Desert Dunes*. London, UK: Methuen, 1941.

[4] A. Rosato, K. J. Strandburg, F. Prinz, and R. H. Swendsen, "Why the Brazil nuts are on top: Size segregation of particulate matter by shaking," *Physical Review Letters*, vol. 58, no. 10, pp. 1038–1040, 1987.

[5] T. Shinbrot and F. J. Muzzio, "Reverse buoyancy in shaken granular beds," *Physical Review Letters*, vol. 81, no. 20, pp. 4365–4368, 1998.

[6] F. W. Von Batchelder and H. E. Stauss, "A method for annealing metal powders without sintering," *Review of Scientific Instruments*, vol. 22, no. 6, pp. 396–397, 1951.

[7] H. M. Jaeger, S. R. Nagel, and R. P. Behringer, "Granular solids, liquids, and gases," *Reviews of Modern Physics*, vol. 68, no. 4, pp. 1259–1273, 1996.

[8] D. Blackmore, R. Samulyak, and A. Rosato, "New mathematical models for particle flow dynamics," *Journal of Nonlinear Mathematical Physics*, vol. 6, no. 2, pp. 198–221, 1999.

[9] I. G. Shatalova, N. S. Gorbunov, and V. I. Likhtman, *Physicochemical Principles of Vibratory Compacting*, vol. 2, ch. 7-206. New York, NY, USA: Plenum Press, 1967.

[10] J. J. Hauth, *Vibrational Compaction of Nuclear Fuels*, vol. 2, pp. 253–276. New York, NY, USA: Plenum Press, 1967.

[11] Y.-J. Lin, "Granular anode for metal-air fuel cell battery." US Patent Application 2004/0023112, 2004.

[12] J. T. Black and R. A. Kohser, *DeGarmo's Materials and Processes in Manufacturing*. Hoboken: Wiley, 10 ed., 2008.

[13] D. J. D'Appolonia and E. D'Appolonia, "Determination of the maximum density of cohesionless soils," in *3rd Asian Regional Conference on Soil Mechanics and Foundation Engineering*, Jerusalem, Israel: Jerusalem Academic Press, 1967.

[14] R. Dobry and R. V. Whitman, *Compaction of Sand on a Vertically Vibrating Table*. American Society for Testing and Materials, 1973.

[15] D. A. Stewart, *The Design and Placing of High Quality Concrete*. London, UK: Spon Press, 1951.

[16] P. E. Evans and R. S. Millman, *The Vibratory Packing of Powders*, vol. 2, pp. 237–251. New York, NY, USA: Plenum Press, 1967.

[17] N. Zhang and A. D. Rosato, "Experiments and simulations on vibration induced densification of bulk solids," *KONA: Powder and Particle Journal*, vol. 24, pp. 93–103, 2006.

[18] R. K. McGeary, *Mechanical Packing of Spherical Particles*, vol. 2, pp. 209–236. New York, NY, USA: Plenum Press, 1967.

[19] T. G. O. Berg, R. L. McDonald, and R. J. Trainor Jr, "The packing of spheres," *Powder Technology*, vol. 3, no. 1, pp. 183–188, 1969.

[20] F. A. Rocke, "The cylindrically ordered packing of equal spheres," *Powder Technology*, vol. 4, no. 4, pp. 180–186, 1971.

[21] J. Duran, T. Mazozi, E. Clement, and J. Rajchenbach, "Decompaction modes of a two-dimensional sandpile under vibration: Model and experiments," *Physical Review E*, vol. 50, no. 4, pp. 3092–3099, 1994.

[22] S. F. Edwards and R. B. S. Oakeshott, "Theory of powders," *Physica A*, vol. 157, no. 3, pp. 1080–1090, 1989.

[23] A. Mehta and S. F. Edwards, "A phenomenological approach to relaxation in powders," *Physica A*, vol. 168, no. 2, pp. 714–722, 1990.

[24] R. B. S. Oakeshott and S. F. Edwards, "Local theory of the statistics of sphere packings," *Physica A*, vol. 189, no. 12, pp. 188–207, 1992.

[25] G. C. Barker and A. Mehta, "Transient phenomena, self-diffusion, and orientational effects in vibrated powders," *Physical Review E*, vol. 47, no. 1, pp. 184–188, 1993.

[26] D. C. Hong, S. Yue, J. K. Rudra, M. Y. Choi, and Y. W. Kim, "Granular relaxation under tapping and the traffic problem," *Physical Review E*, vol. 50, no. 5, pp. 4123–4135, 1994.

[27] J. B. Knight, C. G. Fandrich, C. N. Lau, H. M. Jaeger, and S. R. Nagel, "Density relaxation in a vibrated granular material," *Physical Review E*, vol. 51, no. 5, pp. 3957–3963, 1995.

[28] S. J. Linz, "Phenomenological modeling of the compaction dynamics of shaken granular systems," *Physical Review E*, vol. 54, no. 3, pp. 2925–2930, 1996.

[29] E. R. Nowak, J. B. Knight, E. Ben-Naim, H. M. Jaeger, and S. R. Nagel, "Density fluctuations in vibrated granular materials," *Physical Review E*, vol. 57, no. 2, pp. 1971–1982, 1998.

[30] P. Ribière, P. Philippe, P. Richard, R. Delannay, and D. Bideau, "Slow compaction of granular systems," *Journal of Physics Condensed Matter*, vol. 17, no. 24, pp. S2743–S2754, 2005.

[31] P. Ribière, P. Richard, R. Delannay, D. Bideau, M. Toiya, and W. Losert, "Effect of rare events on out-of-equilibrium relaxation," *Physical Review Letters*, vol. 95, no. 26, 2005.

[32] E. R. Nowak, J. B. Knight, M. L. Povinelli, H. M. Jaeger, and S. R. Nagel, "Reversibility and irreversibility in the packing of vibrated granular material," *Powder Technology*, vol. 94, no. 1, pp. 79–83, 1997.

[33] O. R. Walton and R. L. Braun, "Viscosity, granular-temperature, and stress calculations for shearing assemblies of inelastic, frictional disks.," *Journal of Rheology*, vol. 30, no. 5, pp. 949–980, 1985.

[34] Y. Zhang and P. Cundall, "Numerical simulation of slow deformations," *Proceedings of the U.S. National Congress of Applied Mechanics*, pp. 347–349, 1986.

[35] C. Henrique, G. Batrouni, and D. Bideau, "Effect of boundary conditions on diffusion in two-dimensional granular gases," *Physical Review E*, vol. 63, no. 1 I, pp. 0113011–0113018, 2001.

[36] O. R. Walton and R. L. Braun, "Stress calculations for assemblies of inelastic speres in uniform shear," *Acta Mechanica*, vol. 63, no. 1-4, pp. 73–86, 1986.

[37] M. J. Sweetman, *Addition of a Chain-Cell Search Method and a Van der Waals Force Model to a Particle Dynamics Code*. PhD thesis, NJIT, Newark, NJ, USA, 2003.

[38] H.-J. Kim, *Particle Dynamics Modeling of Boundary Effects in Granular Couette Flow*. PhD thesis, NJIT, Newark, NJ, USA, 1992.

[39] V. Ratnaswamy, A. D. Rosato, D. Blackmore, X. Tricoche, N. Ching, and L. Zuo, "Evolution of solids fraction surfaces in tapping: Simulation and dynamical systems analysis," *Granular Matter*, vol. 14, no. 2, pp. 163–168, 2012.